**Universität Stuttgart**

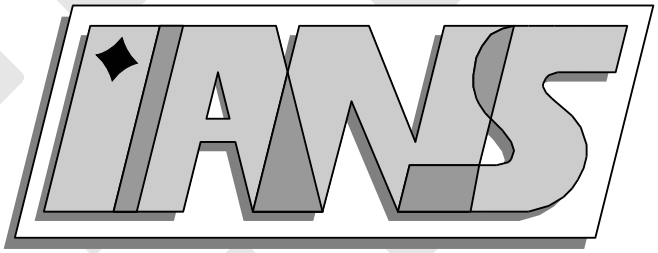

# Reduced Basis Approximation for Nonlinear Parametrized Evolution Equations based on Empirical Operator Interpolation

Martin Drohmann, Bernard Haasdonk, Mario Ohlberger

**Berichte aus dem Institut für Angewandte Analysis und Numerische Simulation**

Preprint 2010/012

**Universität Stuttgart**

# Reduced Basis Approximation for Nonlinear Parametrized Evolution Equations based on Empirical Operator Interpolation

Martin Drohmann, Bernard Haasdonk, Mario Ohlberger

**Berichte aus dem Institut für Angewandte Analysis und Numerische Simulation**

Preprint 2010/012

Institut für Angewandte Analysis und Numerische Simulation (IANS)
Fakultät Mathematik und Physik
Fachbereich Mathematik
Pfaffenwaldring 57
D-70 569 Stuttgart

**E-Mail:** ians-preprints@mathematik.uni-stuttgart.de
**WWW:** http://preprints.ians.uni-stuttgart.de

ISSN **1611-4176**

# REDUCED BASIS APPROXIMATION FOR NONLINEAR PARAMETRIZED EVOLUTION EQUATIONS BASED ON EMPIRICAL OPERATOR INTERPOLATION*

MARTIN DROHMANN†, BERNARD HAASDONK‡, AND MARIO OHLBERGER†

**Abstract.** We present a new approach to treat nonlinear operators in reduced basis approximations of parametrized evolution equations. Our approach is based on empirical interpolation of nonlinear differential operators and their Fréchet derivatives. Efficient offline/online decomposition is obtained for discrete operators that allow an efficient evaluation for a certain set of interpolation functionals. An a posteriori error estimate for the resulting reduced basis method is derived and analyzed numerically. The approach is applied to nonlinear parabolic and hyperbolic equations based on explicit or implicit finite volume discretizations. We show that the resulting reduced scheme is able to capture the evolution of both smooth and discontinuous solutions. In case of symmetries of the problem, the approach realizes an automatic and intuitive space-compression or even space-dimensionality reduction. We perform empirical investigations of the error convergence and runtimes. In all cases we obtain a good runtime acceleration that grows with the problem's size.

**Key words.** model reduction, parametrized evolution equations, reduced basis methods, empirical interpolation, a posteriori error estimation

**AMS subject classifications.** 65M08, 65M15, 65J15, 35L90, 35K90

**1. Introduction.** The numerical solution of parametrized partial differential equations can be a very time-consuming task if many parameter constellations have to be simulated by high-resolution schemes. Such scenarios may occur in parameter studies, optimization, control, inverse problems or statistical analysis of a given parametrized problem. Reduced Basis (RB) methods allow to produce fast reduced models that are good surrogates for the original numerical scheme and allow parameter variations. These methods have gained increasing attention in recent years for stationary elliptic, instationary parabolic problems and various systems. In this contribution, we address the task of model reduction for parametrized evolution equations. These are problems which are characterized by a parameter vector $\boldsymbol{\mu} \in \mathcal{P}$ from some set of possible parameters $\mathcal{P} \subset \mathbb{R}^p$. For a given $\boldsymbol{\mu}$ the evolution problem consists of determining $u(x,t;\boldsymbol{\mu})$ on a bounded domain $\Omega \subset \mathbb{R}^d$ and finite time interval $t \in [0,T], T > 0$ such that

$$\partial_t u(t;\boldsymbol{\mu}) + \mathcal{L}(t,\boldsymbol{\mu})\left[u(t;\boldsymbol{\mu})\right] = 0, \quad u(0;\boldsymbol{\mu}) = u_0(\boldsymbol{\mu}), \tag{1.1}$$

and suitable boundary conditions are satisfied. Here $u_0(\boldsymbol{\mu})$ are the parameter dependent initial values and $\mathcal{L}(t,\boldsymbol{\mu})$ is a parameter dependent spatial differential operator. The initial value and the solution are supposed to have some spatial regularity $u_0(\boldsymbol{\mu}), u(t;\boldsymbol{\mu}) \in \mathcal{W} \subset L^2(\Omega)$.

Evolution schemes produce discrete solutions $u_h^k(\boldsymbol{\mu}) \in \mathcal{W}_h, k = 0,\dots,K$ in an $H$-dimensional discrete space $\mathcal{W}_h \subset L^2(\Omega)$ approximating $u(t^k,\boldsymbol{\mu})$ at the time instants $0 = t^0 < t^1 < \ldots < t^K = T$. These high-dimensional, detailed simulations are

*This work was supported by German Science Foundation (DFG) under the contract number OH 98/2-1.

†Institute of Numerical and Applied Mathematics, University of Münster, 48149 Münster, Germany (mdrohmann@uni-muenster.de). Questions, comments, or corrections to this document may be directed to that email address.

‡Institute of Applied Analysis and Numerical Simulation, University of Stuttgart, 70569 Stuttgart, Germany. The second author was supported by the Baden Württemberg Stiftung gGmbH.

frequently expensive to compute due to the high space resolution and not suitable for use in multi-query settings, i.e. multiple simulation requests with varying parameters $\boldsymbol{\mu}$.

Reduced Basis (RB) methods are increasingly popular methods to solve such parametrized problems, aiming at reduced simulation schemes, which approximate the detailed solutions $u_h^k(\boldsymbol{\mu})$ by efficiently computed reduced solutions $u_{\text{red}}^k \in \mathcal{W}_{\text{red}}$. Here $\mathcal{W}_{\text{red}} \subset L^2(\Omega)$ is an $N$-dimensional reduced basis space with suitable reduced basis $\Phi_N$. The latter is generated in a problem specific way based on snapshots. In particular, reduced basis methods have been applied successfully for various elliptic and parabolic problems, mainly based on finite element discretizations. For linear elliptic problems we refer to [21], linear parabolic equations are treated in [11], extensions to nonlinear equations [23, 9] or systems [22] have also been developed. For reduced methods based on finite volume discretizations we refer to [15].

In this contribution, we develop a new reduced basis framework for a general nonlinear partial differential equations. The approach is applicable to a large class of discretization schemes that are based on evaluations of discretized operators and their directional derivatives only. We exemplify our approach for finite volume schemes where Newton iterations are used for the solution of the resulting non-linear systems. The main ingredient that allows to guarantee this extent of generality is the empirical operator interpolation for discrete operators and their directional derivatives. A further trail of our extension is the derivation of a new a posteriori error estimate that can used for error control and - in particular - to speed up the basis construction procedure in the offline phase of the reduced algorithm.

The idea of empirical interpolation was first proposed for data functions in [2] and used for reduced methods for elliptic and parabolic problems in [10, 19, 9, 3]. Preliminary results of the empirical operator interpolation for purely explicit operators were presented in [16, 7]. In the context of model reduction with POD-methods, empirical interpolation for nonlinear finite difference matrices and their Jacobians was introduced in [5].

The structure of our paper is as follows: Section 2 introduces the empirical operator interpolation in full generality and explains its application on directional derivatives of discrete operators. As already mentioned, this is the key ingredient of our generalized reduced basis approach. In §3 a numerical scheme for evolution schemes is formulated including explicit and implicit contributions both depending nonlinearly on the solution. This scheme is the foundation for the reduced basis scheme presented in §4. We elaborate on the generation of the reduced basis space by the "POD-greedy" algorithm and on the nature and the costs of the offline/online-decomposition. A new a posteriori error estimator is derived in §5. In the experimental Section §6 we demonstrate the applicability of the resulting method for both smooth and discontinuous data subject to nonlinear convection and diffusion. Experimentally, we investigate the approximation properties and demonstrate the runtime gain compared to the full finite volume schemes. We conclude in §7.

**2. Operator Approximation by Empirical Interpolation.** The reduced basis method requires the underlying numerical scheme to be written in a *separable* form allowing efficient decomposition of parameter dependent scalar functionals and precomputed parameter-independent operator parts. Therefore, we now introduce the empirical operator interpolation in order to approximate a - linear or nonlinear - parametrized discrete operator with a surrogate in a *separable* form suitable for efficient evaluations in a reduced basis scheme. The empirical interpolation method

for operators as presented in this section gives rise to a reduced basis framework applicable for a very general class of numerical schemes for evolution equations. The operator based approach gives us the opportunity to rewrite numerical schemes by substituting the spatial operators with their empirical interpolants and to develop reduced schemes based on the high dimensional ones. For details we refer to Sections 3 and 4 below. In §2.1 we show that also the directional derivative of a discrete operator can be interpolated efficiently.

Before we start with the description of the empirical operator interpolation, we introduce some notation used throughout this paper.

**Notation:** We write $\mathcal{W}_h$ for a discrete function space defined on a closed subset $\Omega \subset \mathbb{R}^n$ with a non empty interior and a polygonal boundary. Following the notation of a finite element by P.G. Ciarlet [6], we define the set $\Sigma_h := \{\tau_i\}_{i=1}^H \subset \mathcal{W}_h'$ of linearly independent functionals, which are unisolvent on $\mathcal{W}_h$ such that there exist unique functions $\psi_i \in \mathcal{W}_h, i = 1, \dots, H$ which satisfy

$$\tau_j(\psi_i) = \delta_{ij}, \quad 1 \leq j \leq H.$$

The linear functionals $\tau_i, i = 1, \dots, H$ are called the *degrees of freedom* (DOFs) of the discrete function space $\mathcal{W}_h$ and the functions $\psi_i, i = 1, \dots, H$ are called *basis functions*. Note, that these basis functions can e.g. be finite element, finite volume or discontinuous Galerkin basis functions on a numerical grid $\mathcal{T}_h \subset \Omega$.

We proceed to discretizations of (1.1) which is why from now on, $\mathcal{L}_h(t; \boldsymbol{\mu})$ always denotes a discretized (non-linear) operator acting on an $H$-dimensional discrete function space $\mathcal{W}_h$. In order to decompose the computations in an efficient online and an offline phase for high-dimensional data, the scheme must be formulated in a separable way, i.e. the discrete operators are written as a sum of products of efficiently computable parameter dependent functionals and high-dimensional basis functions that can be precomputed during the offline phase. Hence, we approximate the discrete operators by a separable interpolant $\mathcal{I}_M[\mathcal{L}_h]$ of the form

$$\mathcal{I}_M\left[\mathcal{L}_h(t; \boldsymbol{\mu})\right][u_h] := \sum_{m=1}^{M} l_m\left(\mathcal{L}_h(t; \boldsymbol{\mu})[u_h]\right) \xi_m \approx \mathcal{L}_h(t; \boldsymbol{\mu})[u_h] \tag{2.1}$$

for all $u_h \in \mathcal{W}_h$ with a parameter independent but space dependent *collateral reduced basis* $\boldsymbol{\xi}_M := \{\xi_m\}_{m=1}^M \subset \mathcal{W}_H$ and functionals $l_m : \mathcal{W}_H \to \mathbb{R}$, which must be computable with complexity independent of $H$. The sum is assumed to contain few terms, i.e. $M \ll H$. Such a separable approximation is obviously fully specified by defining the basis functions $\xi_m$, and the functionals $l_m, m = 1, \dots, M$. One can think of many reasonable choices for basis functions and corresponding coefficient functionals, but we focus on a specification resulting in the *empirical operator interpolation*.

**2.1. Empirical Operator Interpolation.** In this section, we adapt the empirical interpolation method introduced for functions in [2] for discretized operators. Firstly, we specify the generation of the collateral reduced basis space and the coefficient functionals. Secondly, we show that the functionals can be computed efficiently, i.e. with complexity independent of the discrete function space dimension $H$. As a further extension, we show that the Fréchet derivative of a discrete operator can be efficiently approximated with the same collateral reduced basis as the operator itself.

**Collateral basis generation.** The method can briefly be expressed based on a set of interpolation DOFs $\Sigma_M := \{\tau_m^{EI}\}_{m=1}^M \subset \Sigma_h$ and a corresponding nodal

**Algorithm 2.1** Collateral reduced basis generation

**INPUT:** $L_{\text{train}}, \varepsilon_{\text{tol}}, M_{\max}$
**OUTPUT:** $\Sigma_M = \left\{\tau_i^{EI}\right\}_{i=1}^{M}, \mathbf{Q}_M = \{q_i\}_{i=1}^{M}$
$M \leftarrow 1$
**repeat**
**for** $u_h \in L_{\text{train}}$ **do**
*1. Compute interpolation coefficients* $\boldsymbol{\sigma}^M(u_h) := \left(\sigma_j^M(u_h)\right)_{j=1}^{M} \in \mathbb{R}^M$ *by solving the linear equation system*

$$\sum_{j=1}^{M} \sigma_j^M(u_h)\tau_i^{EI}[q_j] = \tau_i^{EI}[u_h], \quad i = 1, \ldots, M$$

**end for**
*2. Find approximation with worst error*
$u_M \leftarrow \arg\sup_{u_h \in L_{\text{train}}} \left\| u_h - \sum_{j=1}^{M} \sigma_j^M(u_h) q_j \right\|.$
– *Compute the residual between* $u_M$ *and its current interpolant.*
$r_M \leftarrow u_M - \sum_{j=1}^{M} \sigma_j^M(u_M) q_j$
– *Find interpolation DOF maximizing the residual.*
$\tau_M^{EI} \leftarrow \arg\sup_{\tau \in \Sigma_h} |\tau(r_M)|$
– *Normalize to obtain a new collateral reduced basis function.*
$q_M \leftarrow \frac{r_M}{\tau_M^{EI}(r_M)}$
$M \leftarrow M + 1$
**until** the residual's norm falls below the tolerance $\varepsilon_{\text{tol}} > 0$ or the maximum number of extension steps $M_{\max}$ is reached.

interpolation basis $\boldsymbol{\xi}_M$, i.e. $\tau_{m'}^{EI}[\xi_m] = \delta_{m,m'}$ for $1 \leq m, m' \leq M$. The generation process for these components works analogously to the algorithms described in the original empirical interpolation paper [2].

Algorithm 2.1 is a sketch of how to construct the empirical interpolation components for a finite set of precomputed operator "snapshots" $L_{\text{train}}$. This set should cover the "interesting" dynamics of the operator. A reasonable choice for the training set is

$$L_{\text{train}} := \left\{ \mathcal{L}_h(t^{k_i}; \boldsymbol{\mu}_i) \left[ u_h^{k_i}(\boldsymbol{\mu}_i) \right] \right\}_{i \in I_{\text{train}}}$$

with time-instants $t^{k_i}$ and parameters $\boldsymbol{\mu}_i$ indexed by a suitable finite index set $I_{\text{train}}$. In every of the $M$ iterations the greedy search algorithm determines the worst approximated snapshot in $L_{\text{train}}$ and extracts a new basis vector and interpolation functional from its interpolation residual.

REMARK 2.1. *The nodal basis* $\boldsymbol{\xi}_M$ *is constructed from a basis* $\mathbf{Q}_M := \{q_m\}_{m=1}^{M}$ *made out of basis functions with a different structure, such that* $\tau_m^{EI}[q_m] = 1$ *and* $\tau_{m'}^{EI}[q_m] = 0$ *for all* $m' > m$. *Unlike the nodal basis,* $\mathbf{Q}_M$ *can be constructed iteratively, such that* $\mathbf{Q}_{M-1} \subset \mathbf{Q}_M$. *The nodal basis* $\boldsymbol{\xi}_M$, *however, allows a simpler exposition of the functionals, and can be efficiently constructed from* $\mathbf{Q}_M$, *as the column matrix of basis vectors* $q_m, m = 1, \ldots, M$ *has lower-triangular shape. Therefore, in the following paragraphs we prefer to use* $\boldsymbol{\xi}_M$ *in the exposition where possible.*

REMARK 2.2. *We mention, that the loop over the training set* $L_{train}$ *in Algorithm 2.1, i.e. steps* 1. *and* 2. *in the algorithm can be executed in parallel with no communi-*

*cation costs, such that the offline computation time can be extremely improved by use of parallel hardware.*

**Evaluation of interpolation functionals $\tau_m^{EI} \circ \mathcal{L}_h$.** An efficient evaluation of the functionals $\tau_m^{EI}\left(\mathcal{L}_h(\boldsymbol{\mu})\left[u_h\right]\right)$ for every $\boldsymbol{\mu} \in \mathcal{P}$ requires it to depend on few basis functions only. This fact inspires the following definition.

DEFINITION 2.3 ($H$-independent DOF dependence). *A discrete operator $\mathcal{L}_h : \mathcal{W}_h \to \mathcal{W}_h$ fulfills an $H$-*independent DOF dependence*, if there exists a constant $C \ll H$ such that for all $\tau \in \Sigma_h$ a restriction operator $\mathcal{R}_\tau^C : \mathcal{W}_h \to \mathcal{W}_h, u_h = \sum_{i=1}^H \tau_i(u_h)\psi_i \mapsto \sum_{j \in I_\tau} \tau_j(u_h)\psi_j$ exists that restricts the operator argument to $|I_\tau| \leq C$ degrees of freedom and the equation*

$$\tau\left(\mathcal{L}_h\left[u_h\right]\right) = \tau\left(\mathcal{L}_h\left[\mathcal{R}_\tau^C\left[u_h\right]\right]\right)$$

*still holds for all $u_h \in \mathcal{W}_h$.*

REMARK 2.4. *In particular, finite element or finite volume operators fulfill the $H$-independent DOF dependence, as a point evaluation of an operator application only requires data of the argument on neighbouring grid cells together with geometric information of this subgrid.*

Assuming this $H$-independence condition on a parametrized discrete operator, we formulate its empirical interpolation with exact approximation of operator evaluations by interpolation functionals. This result is summarized in the following observation.

COROLLARY 2.5. *Let $\mathcal{L}_h : \mathcal{P} \times \mathcal{W}_h \to \mathcal{W}_h$ be a parametrized discrete operator fulfilling an $H$-*independent DOF dependence *for all $\mu \in \mathcal{P}$ and let $\Sigma_M$ and $\boldsymbol{\xi}_M$ be determined for this operator by Algorithm 2.1. Then, the empirical operator interpolation $\mathcal{I}_M$ defined by*

$$\mathcal{I}_M\left[\mathcal{L}_h(\boldsymbol{\mu})\left[u_h\right]\right] := \sum_{m=1}^{M} \tau_m^{EI}\left(\mathcal{L}_h(\boldsymbol{\mu})\left[u_h\right]\right)\xi_m \tag{2.2}$$

*gives a separable approximation of $\mathcal{L}_h$ depending on at most $CM$ degrees of freedom for each evaluation.*

Ignoring the parameter independent collateral basis functions, an evaluation of the empirical interpolant has a complexity independent of the dimension $H$. This fact holds during a reduced basis simulation, because then all contributions depending on the collateral reduced basis have already been precomputed and reduced to vectors or matrices with dimensions independent of $H$.

**Evaluation of functionals for the Fréchet derivative $\mathbf{D}\mathcal{L}_h(\boldsymbol{\mu})|_{u_h}\left[v_h\right]$.** Most solvers for numerical approximations of nonlinear partial differential equations use the Newton method to resolve the nonlinearities in the equation and therefore depend on derivatives of discrete operators. It is easy to observe that the Fréchet derivative can also be applied to the empirical interpolant of an operator $\mathcal{L}_h$ as

$$\mathbf{D}\mathcal{I}_M\left[\mathcal{L}_h(\boldsymbol{\mu})\right]|_{u_h}\left[\cdot\right] = \sum_{m=1}^{M} \mathbf{D}\left(\tau_m^{EI} \circ \mathcal{L}_h(\boldsymbol{\mu})\right)|_{u_h}\left[\cdot\right]\xi_m. \tag{2.3}$$

For an efficient usage of such an interpolation in a reduced scheme, it suffices to show that the functionals $\mathbf{D}\tau_m^{EI} \circ \mathcal{L}_h(\boldsymbol{\mu})|_{u_h}$ can be evaluated efficiently: With the

chain rule for Fréchet derivatives and the existence of the derivatives w.r.t. the degrees of freedom, we obtain

$$\mathbf{D}\left(\tau_m^{EI} \circ \mathcal{L}_h(\boldsymbol{\mu})\right)|_{u_h}[v_h] = \sum_{i=1}^{H} \frac{\partial}{\partial \psi_i} \tau_m^{EI}\left(\mathcal{L}_h(\boldsymbol{\mu})[u_h]\right) \tau_i(v_h) \tag{2.4}$$

$$= \sum_{i \in I_{\tau_m}} \frac{\partial}{\partial \psi_i} \tau_m^{EI}\left(\mathcal{L}_h(\boldsymbol{\mu})[u_h]\right) \tau_i(v_h). \tag{2.5}$$

The reduction in the number of summands holds true, as substituting $\tau_m^{EI}\left(\mathcal{L}_h(\boldsymbol{\mu})[u_h]\right)$ with its restriction $\tau_m^{EI}\left(\mathcal{L}_h(\boldsymbol{\mu})\left[\mathcal{R}^C_{\tau_m} u_h\right]\right)$ shows that most of the directional derivatives are zero. Each summand depends on one degree of freedom of the directional function $v_h$ and at most $C$ degrees of freedom of $u_h$ summing up to an overall complexity of $C^2 M \ll H$. Again, this result with all its prerequisites is summarized in the following corollary.

COROLLARY 2.6. *Let $\mathcal{L}_h : \mathcal{P} \times \mathcal{W}_h \to \mathcal{W}_h$ be as in Corollary 2.5 having a Fréchet derivative at the point $u_h \in \mathcal{W}_h$. Then, the Fréchet derivative of the empirical operator interpolation evaluated in direction $v_h \in \mathcal{W}_h$ is an efficiently separable approximation of $\mathbf{D}\mathcal{L}_h(\boldsymbol{\mu})|_{u_h}[v_h]$ with complexity independent of $H$ for all $\boldsymbol{\mu} \in \mathcal{P}$ if the derivatives $\frac{\partial}{\partial \psi_i} l_m(\boldsymbol{\mu})[u_h]$ exist for all $i = 1, \ldots, H$ and $m = 1, \ldots, M$.*

The results of this section allow us to show in §4.3 how the empirical operator interpolation is utilized for the offline/online decomposition of the reduced basis scheme.

**3. Evolution Scheme.** In this section, we define an operator based numerical scheme which can be understood as general formulation for state-of-the-art discretizations of parametrized evolution problems (1.1). As an example, in §3.1 we present how these operators can be specified for a finite volume scheme. Together with the empirical interpolation for discrete operators and their Fréchet derivatives, a reduced scheme will be formulated in §4.

In what follows, we assume a first order discretization in time, and split the space discretization operator into implicit and explicit contributions. Both operator parts may depend nonlinearly on the argument. The non-linear implicit part will be treated by Newton iterations. For clarity of exposition, we fix the time step size, but of course, it would be possible to choose it adaptively in each step.

DEFINITION 3.1 (General parametrized evolution scheme). *Let $\mathcal{W}_h$ be an $H$-dimensional discrete function space with a basis $\{\psi_i\}_{i=1}^H$ and $t^k := k\Delta t, k = 0, \ldots, K$ be a sequence of $K+1$ strictly increasing time instances with a global time step size $\Delta t > 0$. Furthermore, there need to exist a projection $\mathcal{P}_h : L^2(\Omega) \to \mathcal{W}_h$ onto the discrete function space, and we assume an arbitrary space discretization operator $\mathcal{L}_h := \mathcal{L}_I + \mathcal{L}_E$ decomposed in its implicit and explicit contributions $\mathcal{L}_I := \mathcal{L}_I(t^k; \boldsymbol{\mu}), \mathcal{L}_E := \mathcal{L}_E(t^k, \boldsymbol{\mu}) : \mathcal{W}_h \to \mathcal{W}_h$. We define a numerical scheme for discrete solutions $u_h^k := \sum_{i=1}^H u_{h,i}^k \psi_i \in \mathcal{W}_h$ at time instances $t^k$ for $k = 0, \ldots, K$ by initial projection*

$$u_h^0 = \mathcal{P}_h\left[u_0(\boldsymbol{\mu})\right], \tag{3.1}$$

*and subsequently solving the equations*

$$F\left[u_h^{k+1}\right] := (\mathrm{Id} + \Delta t \mathcal{L}_I)\left[u_h^{k+1}\right] - (\mathrm{Id} + \Delta t \mathcal{L}_E)\left[u_h^k\right] = 0, \tag{3.2}$$

*with the Newton-Raphson method. In each Newton step, we solve for the defect* $\delta_h^{k+1,\nu+1}$ *in*

$$\mathbf{D}F|_{u_h^{k+1,\nu}}\left[\delta_h^{k+1,\nu+1}\right] = -F\left[u_h^{k+1,\nu}\right], \tag{3.3}$$

*where* $u_h^{k+1,0} := u_h^k$ *and* $u_h^{k+1,\nu+1} := u_h^{k+1,\nu} + \delta_h^{k+1,\nu+1}$ *define the updates in each Newton step, and the solution at time instance* $t^k$ *is given by* $u_h^{k+1} := u_h^{k+1,\nu_{\max}^k}$. *Here, the last Newton step index* $\nu_{\max}^k$ *equals the smallest integer* $\nu$ *satisfying the inequality*

$$\left\|R_{h,New}^k\right\| \leq \varepsilon^{New} \tag{3.4}$$

*for the Newton residual*

$$R_{h,New}^k := u_h^{k+1} - u_h^k + \Delta t\left(\mathcal{L}_I\left[u_h^{k+1}\right] + \mathcal{L}_E\left[u_h^k\right]\right) \tag{3.5}$$

*and a predefined residual error bound* $\varepsilon^{New} > 0$.

Note that, if $\mathcal{L}_I$ is linear, a single Newton-step is sufficient and in case $\mathcal{L}_I$ is zero, we obtain a purely explicit scheme.

**3.1. Example: nonlinear finite volume scheme.** As special instances of the general evolution equation (1.1), we consider the following scalar nonlinear convection-diffusion problem on a polygonal domain $\Omega \subset \mathbb{R}^2$ with the abbreviation $u = u(t;\boldsymbol{\mu})$ for a clearer exposition:

$$\partial_t u + \nabla\cdot(\mathbf{v}(u;\boldsymbol{\mu})u) - \nabla\cdot(d(u;\boldsymbol{\mu})\nabla u) = 0 \qquad \text{in } \Omega\times[0,T_{\max}] \tag{3.6}$$

with suitable parametrized functions $\mathbf{v}(\cdot;\boldsymbol{\mu}) \in C(\mathbb{R},\mathbb{R}^d)$ and $d(\cdot;\boldsymbol{\mu}) \in C(\mathbb{R},\mathbb{R}^+)$

$$u(0;\boldsymbol{\mu}) = u_0(\boldsymbol{\mu}) \qquad \text{in } \Omega\times\{0\}, \tag{3.7}$$

$$u(\boldsymbol{\mu}) = u_{\text{dir}}(\boldsymbol{\mu}) \qquad \text{on } \Gamma_{\text{dir}}\times[0,T_{\max}], \tag{3.8}$$

$$(\mathbf{v}(u;\boldsymbol{\mu})u - d(u;\boldsymbol{\mu})\nabla u)\cdot\mathbf{n} = u_{\text{neu}}(\boldsymbol{\mu}) \qquad \text{on } \Gamma_{\text{neu}}\times[0,T_{\max}] \tag{3.9}$$

and cyclical boundary conditions on the remaining boundary $\partial\Omega\backslash(\Gamma_{\text{dir}}\cup\Gamma_{\text{neu}})$.

We denote $\mathcal{W}$ as the exact solution space with respect to the space variable that can be chosen e.g. as $L^\infty(\Omega)\cap BV(\Omega) \subset L^2(\Omega)$. We obtain unique entropy solutions in $L^\infty(0,T_{\max};\mathcal{W})$ if the data and boundary functions fulfill adequate regularity conditions. For discussion on well-posedness, uniqueness and existence of entropy solutions, see e.g. [4, 17].

**Numerical scheme.** Before we formulate the numerical scheme, we must introduce some notations. Let $\mathcal{T} := \{e_i\}_{i=1}^H$ denote a numerical grid consisting of $H$ disjoint polygonal elements forming a partition of the domain $\bar{\Omega} = \bigcup_{i=1}^H \bar{e}_i$. For each element $e_i, i = 1,\ldots,H$, we assume that there exist

(i) certain points $x_i$ lying inside the element $e_i$, such that points in adjacent elements are perpendicular to the corresponding edges and

(ii) a set of indices $\mathcal{N}(i) := \mathcal{N}_{\text{in}}(i)\cup\mathcal{N}_{\text{dir}}(i)\cup\mathcal{N}_{\text{neu}}(i)$ counting the element's edges $e_{ij}$ for $j \in \mathcal{N}(i)$, where $\mathcal{N}_{\text{in}}$ corresponds to edges between inner elements of the domain or elements adjacent by cyclical boundary conditions, $\mathcal{N}_{\text{dir}}$ includes those edges on the Dirichlet boundary and $\mathcal{N}_{\text{neu}}$ those ones on the Neumann boundary of the domain.

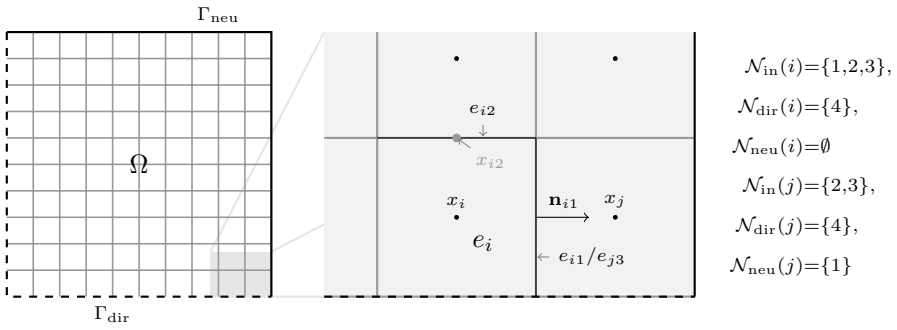


FIGURE 3.1. *Excerpt of a rectangular grid with notations used in this paper.*

On each edge $e_{ij}$, we denote their barycenters by $x_{ij}$ and their outer unit normals by $\mathbf{n}_{ij}$.

The grid enables us to specify a discrete function space $\mathcal{W}_h := \operatorname{span}\{\psi_i\}_{i=1}^H$ spanned by indicator functions $\psi_i := \chi_{e_i}$ piecewise constant on the grid cells. We denote the degrees of freedom of a function $u_h \in \mathcal{W}_h$ by $u_{h,i} = \tau_i(u_h) := u_h(x_i)$. For the time interval discretization, we choose the global time step size $\Delta t$ small enough such that a CFL condition is fulfilled for all parameters $\boldsymbol{\mu} \in \mathcal{P}$.

The implicit and explicit space discretization operator need to model the diffusive respectively the convective dynamics of the underlying partial differential equations. Therefore we define

$$\mathcal{L}_I := \alpha\,\mathcal{L}_{\text{diff}} + \beta\,\mathcal{L}_{\text{conv}}, \tag{3.10}$$

$$\mathcal{L}_E := (1-\alpha)\,\mathcal{L}_{\text{diff}} + (1-\beta)\,\mathcal{L}_{\text{conv}} \tag{3.11}$$

with constants $0 \leq \alpha, \beta \leq 1$ and finite volume operators $\mathcal{L}_{\text{diff}}$ and $\mathcal{L}_{\text{conv}}$ specified below. A judicious choice for the constants is $\alpha = 1$ and $\beta = 0$, because the greater stiffness of diffusion dynamics require implicit discretizations, whereas for instationary problems, it is computationally more efficient to discretize convection terms explictly.

A finite difference approximation of the gradient gives us the DOF-wise definition of the diffusion operator

$$\begin{aligned}(\mathcal{L}_{\text{diff}}[u_h])_i = &-\frac{1}{|e_i|}\sum_{j\in\mathcal{N}_{\text{in}}(i)} \overline{d(u_h;\boldsymbol{\mu})_{ij}}\frac{u_{h,j}-u_{h,i}}{|x_j-x_i|}\\ &-\frac{1}{|e_i|}\sum_{j\in\mathcal{N}_{\text{dir}}(i)} d(u_{\text{dir}}(x_{ij});\boldsymbol{\mu})\frac{u_{\text{dir}}(x_{ij})-u_{h,i}}{2|x_j-x_{ij}|},\end{aligned} \tag{3.12}$$

where $|e_i|$ is the volume of the grid cell $e_i$ and $\overline{d(u_h;\boldsymbol{\mu})_{ij}}$ computes a suitable mean on the edge $e_{ij}$, e.g. the harmonic mean $\frac{2d(u_j)d(u_i)}{d(u_j)+d(u_i)}$. In order to resolve the nonlinearity of the diffusion in a numerical scheme with the Newton-Raphson method, we also

need the operator's directional derivative at a point $u_h$

$$\begin{aligned}\left(\mathbf{D}\mathcal{L}_{\mathrm{diff}}|_{u_h}[v_h]\right)_i = &-\frac{1}{|e_i|}\sum_{j\in\mathcal{N}_{\mathrm{in}}(i)} \mathbf{D}\overline{d(\cdot;\boldsymbol{\mu})_{ij}}|_{u_h}[v_h]\,\frac{u_{h,j}-u_{h,i}}{|x_j-x_i|}\\ &\qquad + \overline{d(u_h;\boldsymbol{\mu})_{ij}}\frac{v_{h,j}-v_{h,i}}{|x_j-x_i|}\\ &-\frac{1}{|e_i|}\sum_{j\in\mathcal{N}_{\mathrm{dir}}(i)} d(u_{\mathrm{dir}}(x_{ij});\boldsymbol{\mu})\frac{-v_{h,i}}{2|x_j-x_{ij}|}.\end{aligned} \tag{3.13}$$

Likewise, we define the finite volume operator for the convection term by

$$\begin{aligned}\left(\mathcal{L}_{\mathrm{conv}}[u_h]\right)_i =&\frac{1}{|e_i|}\sum_{j\in\mathcal{N}_{\mathrm{in}}(i)} g_{ij}(u_{h,i},u_{h,j})\\ &+\frac{1}{|e_i|}\sum_{j\in\mathcal{N}_{\mathrm{dir}}(i)} g_{ij}(u_{h,i},u_{\mathrm{dir}}(x_{ij}))\\ &+\frac{1}{|e_i|}\sum_{j\in\mathcal{N}_{\mathrm{neu}}(i)}\int_{e_i} u_{\mathrm{neu}}\end{aligned} \tag{3.14}$$

with Engquist-Osher flux functions $g_{ij}$ leading to low numerical viscosity in this scheme. The flux functions can be expressed by setting $c_{ij}(u) := \mathbf{n}_{ij}\mathbf{v}(u)u$ for all edges, defining

$$c_{ij}^+(u) := c_{ij}(0) + \int_0^u \max(c_{ij}'(s),0)ds, \qquad c_{ij}^-(u) := \int_0^u \min(c_{ij}'(s),0)ds \tag{3.15}$$

and choosing the flux as $g_{ij}(u,v) := |e_{ij}|\left\{c_{ij}^+(u)+c_{ij}^-(v)\right\}$, cf. [18]. The corresponding directional derivative w.r.t. $v_h$ of the Engquist-Osher flux operator is given by

$$\begin{aligned}\left(\mathbf{D}\mathcal{L}_{\mathrm{conv}}|_{u_h}[v_h]\right)_i =&\frac{1}{|e_i|}\sum_{j\in\mathcal{N}_{\mathrm{in}}(i)} \partial_1 g_{ij}(u_{h,i},u_{h,j})v_{h,i} + \partial_2 g_{ij}(u_{h,i},u_{h,j})v_{h,j}\\ &+\frac{1}{|e_i|}\sum_{j\in\mathcal{N}_{\mathrm{dir}}(i)} \partial_1 g_{ij}(u_{h,i},u_{\mathrm{dir}}(x_{ij}))v_{h,i}.\end{aligned} \tag{3.16}$$

In order to complete the scheme, we can project the initial data onto the discrete function space via a cell averaging operator $\mathcal{P}_h : \mathcal{W} \to \mathcal{W}_h$, DOF-wise defined by $\tau_i\left(\mathcal{P}_h[u_0]\right) := \frac{1}{e_i}\int_{e_i} u_0$ and obtain a specification of the generalized numerical scheme 3.1.

REMARK 3.2 (Restriction to interpolation DOFs). *From the DOF-wise definitions of the operators* (3.13) *and* (3.14) *it follows that a constant number of flops dependent on the maximum number of cell neighbours suffices to numerically compute a single degree of freedom from the operator evaluation result. Therefore, the finite volume operators fulfill the $H$-indepedent DOF dependence condition and are suitable for empirical interpolation with the constant $C$ bounded by one plus the maximum number of edges of an element.*

Note, that the interpolation procedure and the reduced scheme are identically applicable to other evolution problems, discrete function spaces and discretization operators, e.g. finite element or discontinuous Galerkin methods. Hence, for the following development of the reduced basis method, we will express the numerical scheme in terms of the more general notions from Definition 3.1.

**Algorithm 4.1** POD-greedy algorithm

**INPUT:** $M_{\text{train}} \subset \mathcal{P}, \varepsilon_{\text{tol}}, N_{\max}$
**OUTPUT:** $\mathcal{W}_{\text{red}}$
*Initialize reduced basis space:*
$\Phi_{N_0} \leftarrow \{\varphi_n\}_{n=1}^{N_0}$
$N \leftarrow N_0$
**repeat**
1. *Find worst approximated trajectory:*
$\boldsymbol{\mu}_{\max} \leftarrow \arg\max_{\boldsymbol{\mu} \in M_{\text{train}}} \eta(\boldsymbol{\mu})$
2. *Compute trajectory* $\left\{u_h^k(\boldsymbol{\mu}_{\max})\right\}_{k=0}^K$.
3. *Compute new basis function with Galerkin projection* $\mathcal{P}_{\text{red}}$ *projecting onto* $\operatorname{span}\{\varphi_n\}_{n=1}^N$*:*
$\varphi_{N+1} \leftarrow \text{POD}\left(\left\{u_h^k(\boldsymbol{\mu}_{\max}) - \mathcal{P}_{\text{red}}\left[u_h^k(\boldsymbol{\mu}_{\max})\right]\right\}_{k=0}^K\right)$
$N \leftarrow N+1$

**until** the estimate $\eta(\boldsymbol{\mu}_{\max})$ falls beneath a given tolerance $\varepsilon_{\text{tol}}$ or a maximum number of extension steps $N_{\max}$ is reached.
$\mathcal{W}_{\text{red}} \leftarrow \operatorname{span}\{\varphi_n\}_{n=1}^N$

**4. Reduced Basis Method.** The key ingredient for a reduced basis scheme is the availability of a suitable low dimensional reduced basis space $\mathcal{W}_{\text{red}}$. In this section, we give a short review of an algorithm for reduced basis generation. We refer to the article [21] for a more detailed presentation on this topic. In the following §4.2 and §4.3, we introduce a reduced basis scheme for the general evolution problem from Definition 3.1 and comment on its suitability for an efficient offline/online decomposition.

In the experiments, we apply the POD-greedy reduced basis construction method as presented in [15] and a more sophisticated method using adaptive parameter grids introduced in [13]. Different approaches that combine adaptive parameter selection with the generation of multiple reduced basis spaces for different parameter sets have recently been given in [8, 12]. All these methods are inherently accumulative and snapshot-based, like the collateral reduced basis generation schemes described above. Hence, an initially small (or empty) basis is iteratively enriched based on solutions $u_H^{k_i}(\boldsymbol{\mu}_i)$ for certain time steps $k_i$ and parameters $\boldsymbol{\mu}_i$.

**4.1. Reduced basis generation with "POD-greedy".** In order to generate a suitable reduced basis space approximating the manifold of interesting snapshots $\left\{u_h^k(\boldsymbol{\mu}) \in \mathcal{W}_h | \boldsymbol{\mu} \in \mathcal{P}, k = 0, \ldots, K\right\}$, we start with a small initial reduced basis and then perform a greedy search over a finite subset $M_{\text{train}} \subset \mathcal{P}$. This algorithm iteratively extends the reduced basis space by suitable functions from the high dimensional space $\mathcal{W}_h$. Those function are obtained by *(i)* finding the parameter $\boldsymbol{\mu}_{\max} \in M_{\text{train}}$ that is worst approximated by a reduced solution, *(ii)* computing the trajectory $\left\{u_{\text{red}}^k(\boldsymbol{\mu}_{\max})\right\}_{k=0}^K$, and *(iii)* adding the first modes of the proper orthogonal decomposition (POD) for this trajectory's projection error onto the current reduced basis space. These modes can be assumed to reduce the current approximation error of the reduced basis very well. Algorithm 4.1 displays the POD-greedy basis enrichment procedure in compact form (cf. [13]).

In order to assess the quality of reduced simulation trajectories $\left\{u_{\text{red}}^k(\boldsymbol{\mu})\right\}_{k=0}^K$ obtained by a reduced numerical scheme, we assume for any possible reduced basis

space that the reduction error $\|u_{\mathrm{red}}(\boldsymbol{\mu}) - u_h(\boldsymbol{\mu})\|_{L^\infty([0,T_{\max}];\mathcal{W}_h)}$ can be bounded by a function $\eta : \mathcal{P} \to \mathbb{R}$. Of course, it is also possible to use the exact error directly. However, as this direct evaluation depends on a large number of slow and inefficient computations, more efficient a posteriori estimators are preferable. An example for an error estimator separable into parameter independent offline and efficient online computations is given in §5. Alternatively, it would be possible to treat the time instances like parameters and to dispense with the POD step. As the snapshots, however, vary only slightly over time, this strategy would blow both the training set size and the number of error estimator evaluations without gaining much accuracy. The initialization of the reduced basis generation is usually realized by adding initial data projections $\mathcal{P}_h\left[u_0(\boldsymbol{\mu})\right]$. Assuming an affine parameter dependence of the initial data function $u_0$, it is possible to assure that these projections lie in the reduced basis space when it includes all parameter independent contributions.

REMARK 4.1. *Again, we mention that step 1 in Algorithm 4.1 can be distributed into parallel jobs on different cores with no communication costs, as the estimator evaluations $\eta(\boldsymbol{\mu})$ are independent of each other for all $\boldsymbol{\mu} \in M_{train}$.*

**4.2. Reduced Basis Scheme.** In this section we introduce a reduced basis scheme based on the formulation in [16, 14] for explicit discretizations of evolution problems. We extend the scheme by allowing nonlinear or non-separable implicit operator contributions. The basic idea for the reduced basis scheme is to replace the discrete evolution operators $\mathcal{L}_E$ and $\mathcal{L}_I$ from Definition 3.1 by their empirical interpolants $\mathcal{I}_M\left[\mathcal{L}_E\right]$ and $\mathcal{I}_M\left[\mathcal{L}_I\right]$ and applying an orthogonal projection of the numerical scheme onto the reduced basis space $\mathcal{W}_{\mathrm{red}}$ with respect to the scalar product of $\mathcal{W}_h$. For this purpose, we introduce the corresponding orthogonal projection operator $\mathcal{P}_{\mathrm{red}} : \mathcal{W}_h \to \mathcal{W}_{\mathrm{red}}$ satisfying

$$\left\langle \mathcal{P}_{\mathrm{red}}\left[u\right], \varphi \right\rangle = \left\langle u, \varphi \right\rangle \qquad \forall \varphi \in \mathcal{W}_{\mathrm{red}}$$

and define reduced variants of the discrete operators

$$\mathcal{L}_{\mathrm{red},E} := \mathcal{P}_{\mathrm{red}} \circ \mathcal{I}_M \circ \mathcal{L}_E \quad \text{and} \quad \mathcal{L}_{\mathrm{red},I} := \mathcal{P}_{\mathrm{red}} \circ \mathcal{I}_M \circ \mathcal{L}_I. \tag{4.1}$$

We obtain trajectories $\left\{u_{\mathrm{red}}^k\right\}_{k=0}^K$ with snapshots $u_{\mathrm{red}}^k \in \mathcal{W}_{\mathrm{red}}$ for $k = 0, \dots, K-1$ analogously to the evolution scheme described in Definition 3.1. The reduced initial data is given by projection of the initial data

$$u_{\mathrm{red}}^0 := \mathcal{P}_{\mathrm{red}}\left[\mathcal{P}_h\left[u_0\right]\right]. \tag{4.2}$$

Then, for each $k = 0, \dots, K-1$ Newton step solutions are computed by finding for $\nu = 0, \dots, \nu_{\max}^k$ defects $\delta_{\mathrm{red}}^{k+1,\nu}$ solving

$$\begin{aligned}\left(\mathrm{Id} + \Delta t \mathbf{D}\mathcal{L}_{\mathrm{red},I}\big|_{u_{\mathrm{red}}^{k+1,\nu}}\right)\left[\delta_{\mathrm{red}}^{k+1,\nu+1}\right] &= -u_{\mathrm{red}}^{k+1,\nu} + u_{\mathrm{red}}^k \\ &\quad - \Delta t\left[\mathcal{L}_{\mathrm{red},I}\left[u_{\mathrm{red}}^{k+1,\nu}\right] + \mathcal{L}_{\mathrm{red},E}\left[u_{\mathrm{red}}^k\right]\right],\end{aligned} \tag{4.3}$$

with $u_{\mathrm{red}}^{k+1,0} := u_{\mathrm{red}}^k$, $u_{\mathrm{red}}^{k+1,\nu+1} := u_{\mathrm{red}}^{k+1,\nu} + \delta_{\mathrm{red}}^{k+1,\nu+1}$ for $\nu = 1, \dots, \nu_{\max}^k - 1$, and finally assigning the reduced solution for the next time step by

$$u_{\mathrm{red}}^{k+1} := u_{\mathrm{red}}^{k+1,\nu_{\max}(k)}. \tag{4.4}$$

Here, the final Newton iteration index $\nu^k_{max}$ is the smallest integer such that the norm of the residual defined as

$$R^k_{\mathrm{red,New}} := u^{k+1}_{\mathrm{red}} - u^k_{\mathrm{red}} + \Delta t \left(\mathcal{L}_{\mathrm{red},I}\left[u^{k+1}_{\mathrm{red}}\right] + \mathcal{L}_{\mathrm{red},E}\left[u^k_{\mathrm{red}}\right]\right) \tag{4.5}$$

drops below a given tolerance $\varepsilon^{\mathrm{New}}$.

REMARK 4.2. *If $\mathcal{L}_I$ is linear, a single Newton-step is sufficient, if $\mathcal{L}_I$ is zero, no Newton step at all is necessary and the numerical scheme is purely explicit. This case has already been discussed in [16]. Non-linear parabolic problems with finite element discretizations are also discussed in [11, 3] and [10]. Differently from the operator based approach presented in this paper, those reduced basis methods make use of an empirical interpolation applied to specific data functions only.*

For easier analysis of the computational complexity during offline and online phase, we translate the above sketched reduced scheme into a vector-valued formulation based on the few degrees of freedom of the reduced solution.

DEFINITION 4.3 (Reduced basis scheme with empirical operator interpolation). *We assume a numerical scheme from Definition 3.1 with operators $\mathcal{L}_E$ and $\mathcal{L}_I$ fulfilling an $H$-independent DOF dependence. Hence, we can assume that an appropriate empirical interpolation operator $\mathcal{I}_M$ is defined by means of an empirical interpolation basis $\boldsymbol{\xi}_M$ and an enumerated subset of degrees of freedom $\Sigma_M := \left\{\tau^{EI}_m\right\}^M_{m=1} \subset \Sigma_h$. The collateral reduced basis space shall be the same for both the operators $\mathcal{L}_E$ and $\mathcal{L}_I$ (c.f. Remark 4.4). Furthermore, there must be an orthornormal reduced basis $\Phi_N := \{\varphi_n\}^N_{n=1}$ available that spans the reduced basis space $\mathcal{W}_{\mathrm{red}}$.*

*We define the following scheme for sequentially expressing*

(i) *the reduced solution $u^k_{\mathrm{red}}(\boldsymbol{\mu}) := \sum_{n=1}^N a^k_n(\boldsymbol{\mu})\varphi_n$,*
(ii) *intermediate Newton step solutions $u^{k,\nu}_{\mathrm{red}}(\boldsymbol{\mu}) := \sum_{n=1}^N a^{k,\nu}_n \varphi_n$ and*
(iii) *Newton step defects $\delta^{k,\nu}_{\mathrm{red}} := \sum_{n=1}^N d^{k,\nu}_n \varphi_n$*

*by computing the coefficient vectors*

$$\mathbf{a}^k = \left(a^k_1, \ldots, a^k_N\right)^T, \quad \mathbf{a}^{k,\nu} = \left(a^{k,\nu}_1, \ldots, a^{k,\nu}_N\right)^T \text{ and } \mathbf{d}^{k,\nu} = \left(d^{k,\nu}_1, \ldots, d^{k,\nu}_N\right)^T$$

*for $k = 0, \ldots, K$ and $\nu = 0, \ldots, \nu^k_{\max}$:*

*The initial solution vector is obtain by projection onto the reduced basis space*

$$\mathbf{a}^0 := \left(\left(\mathcal{P}_{\mathrm{red}}\left[\mathcal{P}_h[u_0(\boldsymbol{\mu})], \varphi_1\right]\right), \ldots, \left(\mathcal{P}_{\mathrm{red}}\left[\mathcal{P}_h[u_0(\boldsymbol{\mu})], \varphi_N\right]\right)\right)^T. \tag{4.6}$$

*Then, for each time index $k = 0, \ldots, K-1$ we compute Newton iterations by finding defects $\mathbf{d}^{k+1,\nu+1}$ and residuals $\mathbf{r}^{k+1,\nu+1}$ solving for $\nu = 0, \ldots, \nu^k_{\max} - 1$ the equations*

$$\begin{aligned} &\left(\mathrm{Id} + \Delta t \mathbf{C} \mathbf{l}'_I(t^k; \boldsymbol{\mu})\left[\mathbf{a}^{k+1,\nu}\right]\right)\left[\mathbf{d}^{k+1,\nu+1}\right] \\ &\qquad = -\mathbf{a}^{k+1,\nu} + \mathbf{a}^{k+1,0} \\ &\qquad\quad - \Delta t \mathbf{C}\left(\mathbf{l}_I(t^k; \boldsymbol{\mu})\left[\mathbf{a}^{k+1,\nu}\right] + \mathbf{l}_E(t^k; \boldsymbol{\mu})\left[\mathbf{a}^{k+1,0}\right]\right) \end{aligned} \quad , \tag{4.7}$$

$$\begin{aligned} \mathbf{r}^{k+1,\nu+1} &:= \mathbf{a}^{k+1,\nu+1} - \mathbf{a}^{k+1,0} \\ &\quad + \Delta t \mathbf{C}\left(\mathbf{l}_I(t^k; \boldsymbol{\mu})\left[\mathbf{a}^{k+1,\nu+1}\right] + \mathbf{l}_E(t^k; \boldsymbol{\mu})\left[\mathbf{a}^{k+1,0}\right]\right) \end{aligned} \tag{4.8}$$

*with updates*

$$\begin{aligned} \mathbf{a}^{k+1,0} &:= \mathbf{a}^k, \\ \mathbf{a}^{k+1,\nu+1} &:= \mathbf{a}^{k+1,\nu} + \mathbf{d}^{k+1,\nu+1}, \\ \mathbf{a}^{k+1} &:= \mathbf{a}^{k+1,\nu^k_{\max}}. \end{aligned} \tag{4.9}$$

*The number of Newton steps $\nu_{\max}^k$ at each time step is chosen as the smallest integer $\nu$ such that the residual norm drops below the specified tolerance for the Newton scheme, i.e. for which $\left(\left(\mathbf{r}^{k+1,\nu+1}\right)^T \mathbf{M}\mathbf{r}^{k+1,\nu+1}\right)^{\frac{1}{2}} < \varepsilon^{New}$ holds.*

*The utilized vectors and matrices are defined as*

$$(\mathbf{M})_{nn'} := \langle \varphi_n, \varphi_{n'} \rangle = \delta_{nn'}, \tag{4.10}$$

$$(\mathbf{C})_{nm} := \langle \xi_m, \varphi_n \rangle, \tag{4.11}$$

$$\left(\mathbf{l}_I' \left(t^k; \boldsymbol{\mu}\right) \left[\mathbf{a}^{k+1,\nu}\right]\right)_{mn} := \sum_{i=1}^{H} \frac{\partial}{\partial \psi_i} \left(\tau_m^{EI} \circ \mathcal{L}_I(t^k; \boldsymbol{\mu})\right) \left[u_{\text{red}}^{k+1,\nu}\right] \tau_i\left(\varphi_n\right), \tag{4.12}$$

$$\left(\mathbf{l}_I \left(t^k; \boldsymbol{\mu}\right) \left[\mathbf{a}^{k+1,\nu}\right]\right)_m := \tau_m^{EI} \left(\mathcal{L}_I(t^k; \boldsymbol{\mu}) \left[u_{\text{red}}^{k+1,\nu+1}\right]\right), \tag{4.13}$$

$$\left(\mathbf{l}_E \left(t^k; \boldsymbol{\mu}\right) \left[\mathbf{a}^{k}\right]\right)_m := \tau_m^{EI} \left(\mathcal{L}_E(t^k; \boldsymbol{\mu}) \left[u_{\text{red}}^{k}\right]\right) \tag{4.14}$$

*for $n, n' = 1, \ldots, N$ and $m = 1, \ldots, M$.*

REMARK 4.4. *In the reduced basis scheme, we only use one collateral reduced basis space and one set of interpolation DOFs for both the operators $\mathcal{L}_E$ and $\mathcal{L}_I$. This is a feasible choice, whenever the operators implement similar "dynamics". Separate reduced basis spaces would include large redundancies in such scenarios. For a single collateral reduced basis, the training set $L_{train}$ from which the collateral reduced basis functions are generated must simply be extended by operator evaluations of both operators and – apart from that – no modifications of the empirical interpolation algorithm are necessary.*

**4.3. Offline/Online Decomposition.** We now show that the reduced scheme from Definition 4.3 allows a full offline/online decomposition by summarizing the computed data fields and their theoretical complexity and size. The ability to precompute high-dimensional data in a single offline phase, is the key for efficient and fast online simulations.

The high-dimensional output during basis generation consists of

(i) the collateral reduced basis functions $\{\xi_m\}_{m=1}^M \subset \mathcal{W}_h$, corresponding interpolation DOFs $\Sigma_M$ and the global index set $I_M := \bigcup \{I_\tau | \tau \in \Sigma_M\}$ for all operators subject to an empirical interpolation procedure, and

(ii) the reduced basis functions $\{\varphi_n\}_{n=1}^N \subset \mathcal{W}_h$.

For clarity of exposition, we describe the generated data only for one empirical interpolated operator $\mathcal{L}_h$. This is correct for schemes with purely implicit ($\mathcal{L}_h \equiv \mathcal{L}_I$) or purely explicit operator ($\mathcal{L}_h \equiv \mathcal{L}_E$) contributions, but can easily be extended to more complex situations. Before we proceed to reduced simulations, the high-dimensional data must be processed. Assuming that the initial data function is in a separable form, i.e.

$$u_0 = \sum_{q=1}^{Q} \sigma_0^q(\boldsymbol{\mu}) u_0^q \tag{4.15}$$

with parameter dependent functionals $\sigma_0^q$ and parameter independent functions $u_0^q \in \mathcal{W}_h$ for $q = 1, \ldots, Q$, the parameter independent projections $\mathcal{P}_{\text{red}}\left[\mathcal{P}_h\left[u_0^q\right]\right]$ can be precomputed with the already known reduced basis functions. Alternatively, the initial data function can also be included into the collateral reduced basis generation process and be treated analogously to the discretization operators. Efficient evaluations of the operator during the online phase, depend on

(i) restrictions of the reduced basis functions to $\{\mathcal{R}_M[\varphi_n]\}_{n=1}^N$ with a restriction operator

$$\mathcal{R}_M : \mathcal{W}_h \to \mathcal{W}_h, \quad u_h = \sum_{i=1}^{H} \tau_i(u_h)\,\psi_i \mapsto \sum_{i\in I_M} \tau_i(u_h)\,\psi_i \tag{4.16}$$

and

(ii) the gram matrix $\mathbf{C}$ from (4.11), whose entries $C_{nm} = \langle \xi_m, \varphi_n \rangle$ depend on the *nodal* collateral reduced basis functions $\{\xi_m\}_{m=1}^M$ that need to be generated from the functions $\{q_m\}_{m=1}^M$ in a further pre-processing step. Note that this "basis transformation" is very efficient because of the special form of the collateral reduced basis (c.f. Remark 2.1).

REMARK 4.5. *In practice, discretization operators, like finite volume or finite element discretization operators are usually grid-based and the degrees of freedom correspond to distinctive points on the grid cells or its interfaces. In such case, a subgrid $\mathcal{S}_h \subset \mathcal{T}_h \subset \Omega$ might be necessary in order to compute the local operator evaluations and the restriction operator efficiently as illustrated in Figure 4.1).*

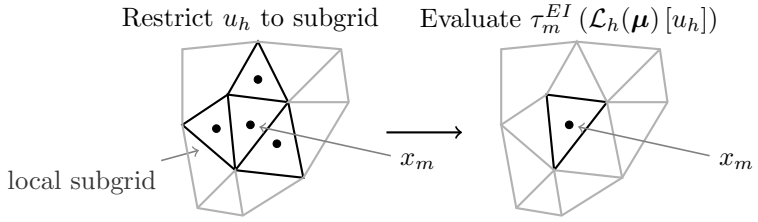


FIGURE 4.1. *Illustration of finite volume operator evaluation on a local subgrid*

With the restricted reduced basis functions the local operator evaluations

$$\left(\tau_m^{EI} \circ \mathcal{L}_h(t^k;\boldsymbol{\mu})\right)\left[\sum_{n=1}^{N} a_n \varphi_n\right] = \left(\tau_m^{EI} \circ \mathcal{L}_h(t^k;\boldsymbol{\mu})\right)\left[\sum_{n=1}^{N} a_n \mathcal{R}_M[\varphi_n]\right] \tag{4.17}$$

have a complexity of $\mathcal{O}(N|I|) = \mathcal{O}(NM)$ for all $m = 1, \ldots, M$. This result can be applied to equations (4.13)-(4.14) and we see, that each of them lies in the complexity class $\mathcal{O}(NM^2)$. The generation of the Jacobian from equation (4.12) depends on $\mathcal{O}(N^2M^2)$ flops. This outreaches all other computations for the assembling of reduced matrices and vectors including matrix-matrix-multiplication of the reduced Jacobian with $\mathbf{C}$ consuming $\mathcal{O}(N^2M)$ flops. Therefore, one Newton step (4.7) of the reduced scheme has complexity $\mathcal{O}(N^2M^2 + N^3)$ including the costs for the linear equation solver. The computation of the Newton residual has costs $\mathcal{O}(N^2M^2)$. Unlike in the detailed simulation steps, the left hand side matrix in the linear equation system is not sparse. Because $N$ is very small compared to the dimension of the detailed numerical scheme, we still expect the solution of the equation system to be much faster. We summarize that the reduced scheme is independent of the high dimensional data size $H$ for each parameter after the offline-phase. A detailed comparison between costs for detailed and reduced simulations is given in Table 4.1.

**5. A posteriori error estimation.** Rigorous a posteriori error estimators can be derived for the error between the reduced and detailed simulation. For a simple

| | detailed simulation | reduced simulation |
|---|---|---|
| Initial data projection | Eqn. (3.1): $\mathcal{O}(H)$ | Eqn. (4.6): $\mathcal{O}(N)$ |
| Assembling of LHS and RHS in Newton step | Eqn. (3.3): $\mathcal{O}(H)$ | Eqn. (4.7): $\mathcal{O}(N^2M^2)$ |
| Solving Newton step | Eqn. (3.3): depending on linear solver, approximately $\mathcal{O}(H^2)$ | Eqn. (4.7): $\mathcal{O}(N^3)$ |
| Computing residual | Eqn. (3.4): $\mathcal{O}(H)$ | Eqn. (4.8): $\mathcal{O}(N^2M^2)$ |

TABLE 4.1
*Comparison of theoretical runtime complexities between detailed and reduced simulations.*

estimator with pure explicit discretization, we refer to [16]. Here, we derive a more accurate estimator which includes implicit discretization and residuals from Newton steps.

THEOREM 5.1. *Let* $\left\{u_h^k(\boldsymbol{\mu})\right\}_{k=0}^K$ *and* $\left\{u_{\mathrm{red}}^k(\boldsymbol{\mu})\right\}_{k=0}^K$ *be solution trajectories obtained via the evolution schemes from Definitions 3.1 and 4.3 where the initial projection onto the reduced basis space is exact, i.e.* $u_h^0(\boldsymbol{\mu}) \in \mathcal{W}_{\mathrm{red}}$ *for all* $\boldsymbol{\mu} \in \mathcal{P}$*. Further, we make two assumptions on the discretization operators* $\mathrm{Id} + \Delta t\mathcal{L}_I$ *and* $\mathrm{Id} - \Delta t\mathcal{L}_E$*. Firstly, the operators need to fulfill a lower respectively an upper Lipschitz continuity condition such that there exist constants* $C_I, C_E > 0$*, and for all* $u, v \in \mathcal{W}_h$ *the inequalities*

$$\|u - v + \Delta t\mathcal{L}_I[u] - \Delta t\mathcal{L}_I[v]\| \geq \frac{1}{C_I}\|u - v\| \tag{5.1}$$

$$\|u - v + \Delta t\mathcal{L}_E[u] - \Delta t\mathcal{L}_E[v]\| \leq C_E\|u - v\| \tag{5.2}$$

*hold. Secondly, we assume the exactness of the empirical interpolation of the operators for a certain number of collateral reduced basis functions, i.e. there exists a positive integer* $M' > 0$*, such that*

$$\mathcal{I}_{M+M'}[\mathcal{L}_I]\left[u_{\mathrm{red}}^k(\boldsymbol{\mu})\right] = \mathcal{L}_I\left[u_{\mathrm{red}}^k(\boldsymbol{\mu})\right] \quad \text{and} \tag{5.3}$$

$$\mathcal{I}_{M+M'}[\mathcal{L}_E]\left[u_{\mathrm{red}}^k(\boldsymbol{\mu})\right] = \mathcal{L}_E\left[u_{\mathrm{red}}^k(\boldsymbol{\mu})\right] \tag{5.4}$$

*for all* $k = 0, \ldots, K$ *and* $\boldsymbol{\mu} \in \mathcal{P}$*. Note, that the last assumption is always fulfilled for* $M + M' = H$ *but for efficiency reasons in practice a much smaller value for* $M'$ *needs to be used.*

*The norm of the error* $e^k := u_h^k(\boldsymbol{\mu}) - u_{\mathrm{red}}^k(\boldsymbol{\mu})$ *can be bounded for* $k = 0, \ldots, K$ *by* $\eta^k$ *which is an efficiently computable function defined by*

$$\left\|e^k\right\| \leq \eta^k := \sum_{i=0}^{k-1} C_I^{k-i+1} C_E^{k-i} \left( \left\| \sum_{m=M}^{M+M'} \Delta t\theta_m^{i+1} q_m \right\| + \varepsilon^{New} + \left\|\Delta t R^{i+1}\right\| \right) \tag{5.5}$$

*with a residual for the error due to the Galerkin projection on the reduced basis space*

$$\Delta t R^{k+1} := \left(\mathrm{Id} + \Delta t\mathcal{I}_M[\mathcal{L}_I]\right)\left[u_{\mathrm{red}}^{k+1}\right] - \left(\mathrm{Id} - \Delta t\mathcal{I}_M[\mathcal{L}_E]\right)\left[u_{\mathrm{red}}^k\right] \tag{5.6}$$

*and empirical interpolation coefficients* $\boldsymbol{\theta}^k := \left\{\theta_m^k\right\}_{m=1}^{M+M'}$ *solving the system of equations*

$$\tau_m^{EI}\left(\mathcal{L}_I\left[u_{\mathrm{red}}^k\right] + \mathcal{L}_E\left[u_{\mathrm{red}}^{k-1}\right]\right) = \sum_{m'=1}^{M+M'} \theta_{m'}^k \tau_m^{EI}(q_{m'}). \tag{5.7}$$

*Proof. First, we check that the residual norm* $\left\|\Delta t R^k\right\|$ *can be computed efficiently, because with Definitions* (5.6), (4.10)-(4.14) *and the empirical interpolation gram matrix* $\mathbf{X}$ *defined by*

$$(\mathbf{X})_{mm'} := \langle \xi_m, \xi_{m'} \rangle \tag{5.8}$$

*it follows that*

$$\begin{aligned}
\Delta t^2 \left\|R^{k+1}\right\|^2 &= \left\langle \Delta t R^{k+1}, \Delta t R^{k+1} \right\rangle \\
&= \left(\mathbf{a}^{k+1} - \mathbf{a}^k\right)^T \mathbf{M} \left(\mathbf{a}^{k+1} - \mathbf{a}^k\right)^T \\
&\quad + 2\Delta t \left(\mathbf{l}_I \left[\mathbf{a}^{k+1}\right] + \mathbf{l}_E \left[\mathbf{a}^k\right]\right)^T \mathbf{C} \left(\mathbf{a}^{k+1} - \mathbf{a}^k\right) \\
&\quad + \Delta t^2 \left(\mathbf{l}_I \left[\mathbf{a}^{k+1}\right] + \mathbf{l}_E \left[\mathbf{a}^k\right]\right)^T \mathbf{X} \left(\mathbf{l}_I \left[\mathbf{a}^{k+1}\right] + \mathbf{l}_E \left[\mathbf{a}^k\right]\right).
\end{aligned}$$

*Let us now derive the error bound. After each Newton iteration in the detailed numerical scheme, we obtain the equation*

$$(\mathrm{Id} + \Delta t \mathcal{L}_I) \left[u_h^{k+1}\right] = (\mathrm{Id} - \Delta t \mathcal{L}_E) \left[u_h^k\right] + R_{h,New}^k \tag{5.9}$$

*with Newton residual* $\left\|R_{h,New}^k\right\| \leq \varepsilon^{New}$.

*The same can be obtained with* (5.6) *for solutions of the reduced numerical scheme*

$$(\mathrm{Id} + \Delta t \mathcal{I}_M [\mathcal{L}_I]) \left[u_{\mathrm{red}}^{k+1}\right] = (\mathrm{Id} - \Delta t \mathcal{I}_M [\mathcal{L}_E]) \left[u_{\mathrm{red}}^k\right] + \Delta t R^{k+1}. \tag{5.10}$$

*Subtracting* (5.9) *from* (5.10) *leads to*

$$\begin{aligned}
&\underbrace{(\mathrm{Id} + \Delta t \mathcal{L}_I) \left[u_h^{k+1}\right] - (\mathrm{Id} + \Delta t \mathcal{I}_M [\mathcal{L}_I]) \left[u_{\mathrm{red}}^{k+1}\right]}_{=:(I)} \\
&\qquad = \underbrace{(\mathrm{Id} - \Delta t \mathcal{L}_E) \left[u_h^k\right] - (\mathrm{Id} - \Delta t \mathcal{I}_M [\mathcal{L}_E]) \left[u_{\mathrm{red}}^k\right]}_{=:(II)} \\
&\qquad\quad + R_{h,New}^{k+1} - \Delta t R^{k+1}.
\end{aligned} \tag{5.11}$$

*After adding zeros to each of* $(I)$ *and* $(II)$*, these can be decomposed into terms that can (a) be estimated with the Lipschitz conditions and are (b) efficiently computable terms, only depending on low dimensional data*

$$\begin{aligned}
(I) = &\underbrace{(\mathrm{Id} + \Delta t \mathcal{L}_I) \left[u_h^{k+1}\right] - (\mathrm{Id} + \Delta t \mathcal{L}_I) \left[u_{\mathrm{red}}^{k+1}\right]}_{=:(Ia)} \\
&+ \underbrace{(\mathrm{Id} + \Delta t \mathcal{L}_I) \left[u_{\mathrm{red}}^{k+1}\right] - (\mathrm{Id} + \Delta t \mathcal{I}_M [\mathcal{L}_I]) \left[u_{\mathrm{red}}^{k+1}\right]}_{=:(Ib)},
\end{aligned} \tag{5.12}$$

$$\begin{aligned}
(II) = &\underbrace{(\mathrm{Id} - \Delta t \mathcal{L}_E) \left[u_h^k\right] - (\mathrm{Id} - \Delta t \mathcal{L}_E) \left[u_{\mathrm{red}}^k\right]}_{=:(IIa)} \\
&+ \underbrace{(\mathrm{Id} - \Delta t \mathcal{L}_E) \left[u_{\mathrm{red}}^k\right] - (\mathrm{Id} - \Delta t \mathcal{I}_M [\mathcal{L}_E]) \left[u_{\mathrm{red}}^k\right]}_{=:(IIb)}.
\end{aligned} \tag{5.13}$$

*Thereby, we have split the error propagation from the error at a previous time step* $(Ia), (IIa)$ *from the error contribution through the empirical interpolation of the explicit and implicit discretization operators* $(Ib), (IIb)$*. Substituting the previous equations into* (5.11)*, bringing* $(Ia)$ *on the left hand side and applying the Lipschitz condition* (5.1) *on it we obtain a bound for the error* $\left\|e^{k+1}\right\|$ *by*

$$\begin{aligned}
\left\|e^{k+1}\right\| &\leq C_I \left\|(\mathrm{Id} + \Delta t \mathcal{L}_I)\left[u_h^{k+1}\right] - (\mathrm{Id} + \Delta t \mathcal{L}_I)\left[u_{\mathrm{red}}^{k+1}\right]\right\| \\
&= C_I \Bigg\| (\mathrm{Id} + \Delta t \mathcal{I}_M\left[\mathcal{L}_I\right])\left[u_{\mathrm{red}}^{k+1}\right] - (\mathrm{Id} + \Delta t \mathcal{L}_I)\left[u_{\mathrm{red}}^{k+1}\right] \\
&\qquad + (\mathrm{Id} - \Delta t \mathcal{L}_E)\left[u_h^k\right] - (\mathrm{Id} - \Delta t \mathcal{L}_E)\left[u_{\mathrm{red}}^k\right] \\
&\qquad + (\mathrm{Id} - \Delta t \mathcal{L}_E)\left[u_{\mathrm{red}}^k\right] - (\mathrm{Id} - \Delta t \mathcal{I}_M\left[\mathcal{L}_E\right])\left[u_{\mathrm{red}}^k\right] \\
&\qquad + R_h^{New} - \Delta t R^{k+1} \Bigg\| \\
&\leq C_I \left\| \sum_{m=M+1}^{M+M'} \Delta t \theta_m^{k+1} q_m \right\| + C_E \left\|e^k\right\| + \varepsilon^{New} + \left\|\Delta t R^{k+1}\right\|,
\end{aligned} \tag{5.14}$$

*where the last inequality uses the Lipschitz continuity* (5.2) *of* $\mathcal{L}_E$*, the exactness assumptions* (5.3) *and* (5.4) *on* $(Ib)$ *respectively* $(IIb)$*, the boundedness of the Newton residuals and the definition of the empirical interpolation coefficients. Resolving the recursion in* (5.14) *with initial error* $\left\|e^0\right\| = 0$ *results in the proposed error bound.*
□

REMARK 5.2. *The Newton iteration error bound* $\varepsilon^{New}$ *is not weighted by the time step size, such that its influence on the estimator grows with the number of time instances. However, this is not a problem as the bound can be chosen arbitrarily small.*

The error estimator (5.5) is similiar to the estimator from [20] for a finite element discretization of the viscous Burger's equation. There, it is proposed to adapt the operator constants $C_E$ and $C_I$ for each parameter by the so-called successive constraints method. This idea can also be transferred to the above described error estimator allowing for better effectivity bounds. A tight bound, especially for the implicit constant $C_I$ is of great importance, because if it is greater than one, the error estimator grows exponentially, otherwise, however, it even ceases over time taking into account that by increasing smoothness through diffusion over time, individual snapshots can better approximate the detailed simulation results.

It is obvious, that the error estimator respects an offline/online decomposition. A preliminary for the separation is the construction of a bigger collateral reduced basis $\boldsymbol{\xi}_{M+M'}$, but in the experimental section, we will observe that only few extra basis functions are needed for reasonable results. The evaluation of the estimator only includes low-dimensional terms or evaluations of the empirically interpolated operators $\mathbf{l}_I$ and $\mathbf{l}_E$. For a detailed discussion on the efficient evalution of these quantities, we refer to §4.3.

**6. Experiments.** In this section, we demonstrate experiments for the presented reduced basis scheme. We consider two model examples that both fit into the setting of example (3.6)-(3.9). The first one is a Burger's problem with a purely explicit discretization. Preliminary results on this example without the new a posteriori error

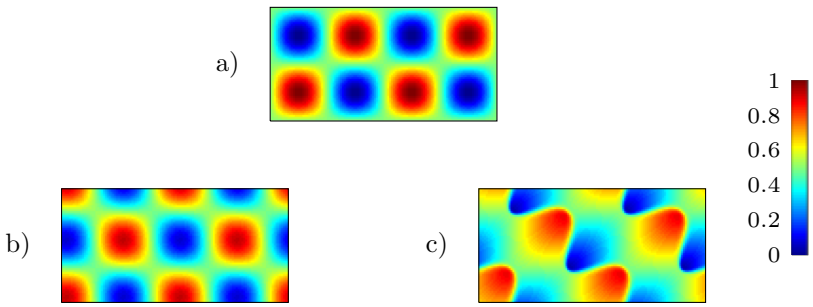


FIGURE 6.1. *Illustration of transport for smooth data. a) Initial data, b) solution at end time for $p = 1$, c) solution at end time for $p = 2$.*

estimator have been presented in [14]. The second problem is based on a nonlinear non-stationary diffusion equation which is discretized purely implicitly. Both problems are nonlinear, but degenerate into linear ones for specific parameter configurations. The second example is also used for an evaluation of the a posteriori error estimator with special focus on its effectivity. The implementation is based on our MATLAB software package *RBmatlab* [1].

**6.1. Burgers equation.** In a first example, we demonstrate the applicability to a nonlinear convection problem

$$\partial_t u - \nabla \cdot f(u) = 0 \tag{6.1}$$

with smooth initial data and a single parameter.

We choose $\Omega = [0, 2] \times [0, 1]$ with purely cyclical boundary conditions and fix the end time $T = 0.3$. We choose the nonlinear flux function $f(u; \boldsymbol{\mu}) := \mathbf{v}u^p$ with exponent $p$ and space- and time-constant velocity field $\mathbf{v} = (1, 1)^T$, the initial data is a smooth function $u_0(x) = \frac{1}{2}(1 + \sin(2\pi x_1)\sin(2\pi x_2))$ for $x = (x_1, x_2)^T \in \Omega$. Overall we consider the single parameter $\boldsymbol{\mu} = (p) \in \mathcal{P} := [1, 2]$ for the exponent in the flux of the evolution equation. We choose a $120 \times 60$ grid for decomposing $\Omega$. The global CFL condition then holds with $K = 100$ timesteps.

Figure 6.1 illustrates the initial data which is independent of the parameter $p$ and the final state for $p = 1$ respectively $p = 2$. The transition between linear convection ($p = 1$) and the nonlinear non-viscous Burgers equation ($p = 2$), can nicely be observed. In the latter case shock discontinuities emerge over the time.

**Offline phase.** For the empirical interpolation of the finite volume discretization operator and the reduced basis, we run Algorithms 2.1 and 4.1, respectively on a workstation computer with 8 cores each running at 2.83 GHz. The implementation of the algorithms makes use of the simple parallelization techniques described in Remarks 2.2 and 4.1. The generation of collateral reduced basis takes 7 minutes and terminates after the maximum dimension $M_{\max} = 350$ for the collateral reduced basis space has been reached. Likewise, the "POD-greedy" algorithm terminates after 16 minutes and produces a reduced basis space of dimension $N_{\max} = 150$. Note, that the main part of the offline run-time costs, namely the search for new basis functions, depends linearly on the number of available cores and therefore, the offline time can be easily controlled by using more processors.

Next, we analyze the quality of the model order reduction induced by the reduced basis spaces. Figure 6.2 helps to understand how the empirical interpolation

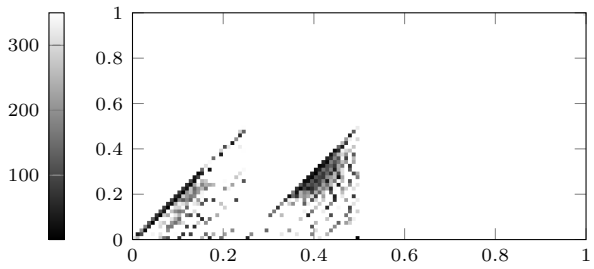


FIGURE 6.2. *Illustration of interpolation DOF selection for Burgers problem. DOFs corresponding to darker points are selected first.*

algorithm actually works. It illustrates the cell midpoints corresponding to the 350 selected interpolation DOFs $\Sigma_M$ and visualizes the selection order of the empirical interpolation algorithm by plotting points selected earlier in darker shades. It is visually comprehensible from the illustration that the algorithm realizes an obvious space compression, because it recognizes the space symmetry of the solution, such that the selected cell midpoints are all located in the lower left quarter of the domain. This means that interpolation DOFs for equivalent solution positions are weighted equally. Furthermore, we see that the first – and therefore most important – interpolation DOFs are lying around the diagonals on which the transportation velocity reaches its maximum and around regions corresponding to the strongest shocks and steepest gradients of the solutions ( c.f. Figure 6.1 c) ). As we expect these interpolation DOFs to give the most distinctive evaluations for different parameters, this observation gives us evidence that the used heuristic for the selection of the collateral reduced basis functions and functionals is a good choice.

**Online phase.** In order to get a notion of the reduced simulations accuracy, in Figure 6.3 we illustrate the error convergence for the resulting reduced simulation scheme. We select a set $M_{\text{test}} \subset \mathcal{P}$ of 20 random values for $p$ not used during basis generation and determine the maximum error $\max_{\boldsymbol{\mu} \in M_{\text{test}}} ||u_N(\boldsymbol{\mu}) - u_H(\boldsymbol{\mu})||_{L^\infty([0,T],L^2(\Omega))}$ between the reduced and the detailed simulations for different dimensionalities $N$ and $M$. The resulting maximum error is plotted in logarithmic scale. The right hand side figure nicely shows, how a simultaneous increase of $N$ and $M$ reveals almost exponential convergence along a selected diagonal of the plot. This simultaneous increase is important: If $M$ is fixed at a low value, increase of $N$ over a certain limit can give an error decrease induced by incorrectly approximated operator evaluations. If $N$ is fixed, raising $M$ gives no error improvement after a certain limit.

The main goal of RB-methods is an accurate approximation under largely reduced simulation time. To assess these computation times, we determine the detailed and reduced simulation times over a sample of 20 random parameters and report the average run-times in Table 6.1. The times were obtained on a workstation computer with 4 cores each running at 2.83 GHz. It can nicely be seen, that we obtain acceleration factors of about 3.5 depending on the dimensionalities of the reduced simulation. Note, that because the reduced simulations are completely independent of the detailed function space $\mathcal{W}_h$, the acceleration factor highly depends on the original problem size. For example, a further test with four times the number of DOFs in $\mathcal{W}_h$ and halved time step size yields a time gain factor of 10 already. Here, the used reduced basis spaces are generated such that they can guarantee the same error between

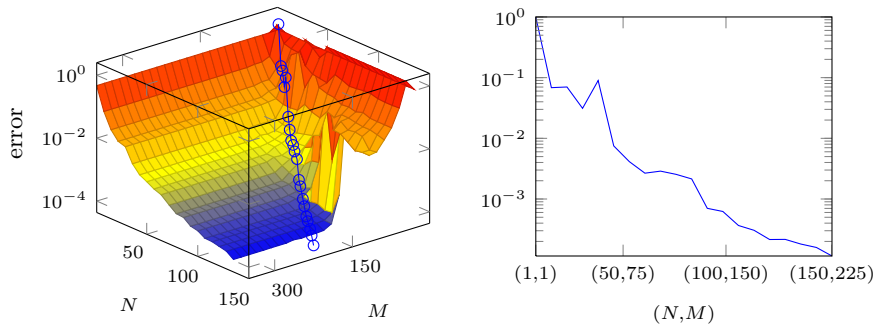


FIGURE 6.3. *Illustration of reduced basis error convergence for continuous initial data with varying dimensionalities $N$ and $M$. The right hand side figure plots the error for simultaneously increased bases sizes $N$ and $M$.*

| Simulation | Dimensionality | Runtime[s] | Error |
|---|---|---|---|
| Detailed | H=7200 | 3.06 | – |
| Reduced | N=30, M=45 | 0.49 | $4.07 \cdot 10^{-2}$ |
| Reduced | N=60, M=90 | 0.58 | $2.97 \cdot 10^{-3}$ |
| Reduced | N=90, M=135 | 0.64 | $5.94 \cdot 10^{-4}$ |
| Reduced | N=120, M=180 | 0.72 | $1.88 \cdot 10^{-4}$ |
| Reduced | N=150, M=225 | 0.76 | $9.30 \cdot 10^{-5}$ |

TABLE 6.1

*Runtime comparison for detailed simulation with reduced simulations of varying reduced dimensionalities. The runtimes and errors are averaged over a test sample of size* 20.

the reduced and the detailed simulations as in the above presented case. The more detailed original simulations also scale down the error to the analytical solution, which we are actually interested in. As this result is conferred to the reduced simulations, the quality of the reduced basis spaces generated from finer detailed simulations, also improves and therefore a direct comparison of the two computed acceleration factors is difficult.

**6.2. Porous Medium Equation.** In this section, we consider the porous medium equation given by the nonlinear diffusion problem

$$\partial_t u - m\Delta u^p = 0 \qquad \text{in } \Omega \times [0, T_{\max}], \tag{6.2}$$

$$u = c_0 \qquad \text{on } \partial\Omega \times [0, T_{\max}], \tag{6.3}$$

$$u(\cdot, 0) = c_0 + u_0 \qquad \text{on } \Omega \times \{0\}\,, \tag{6.4}$$

on a rectangular domain $\Omega = [0,1]^2$. The end time is fixed at $T_{\max} = 1.0$. The initial data function $u_0$ is a field of symmetrically arranged bar shaped concentrations illustrated in Figure 6.4a). This gives us a non-smooth initial concentration depending on the initial parameter $c_0$.

The whole parameter vector is chosen as $\boldsymbol{\mu} = (p, m, c_0) \in \mathcal{P} := [1,5] \times [0, 0.01] \times [0, 0.2]$ such that for $p = 2$ we get the isothermal porous medium equation and for $p > 2$ a porous medium equation with adiabatic flow. For $p = 1$ it degenerates into the linear heat equation. Note also, that for $c_0$ close to zero, diffusion outside the bars is turned off. This effect can be observed in Figure 6.4f)+g) showing large diffusion effects inside the bars with high concentration after short time periods already, but almost

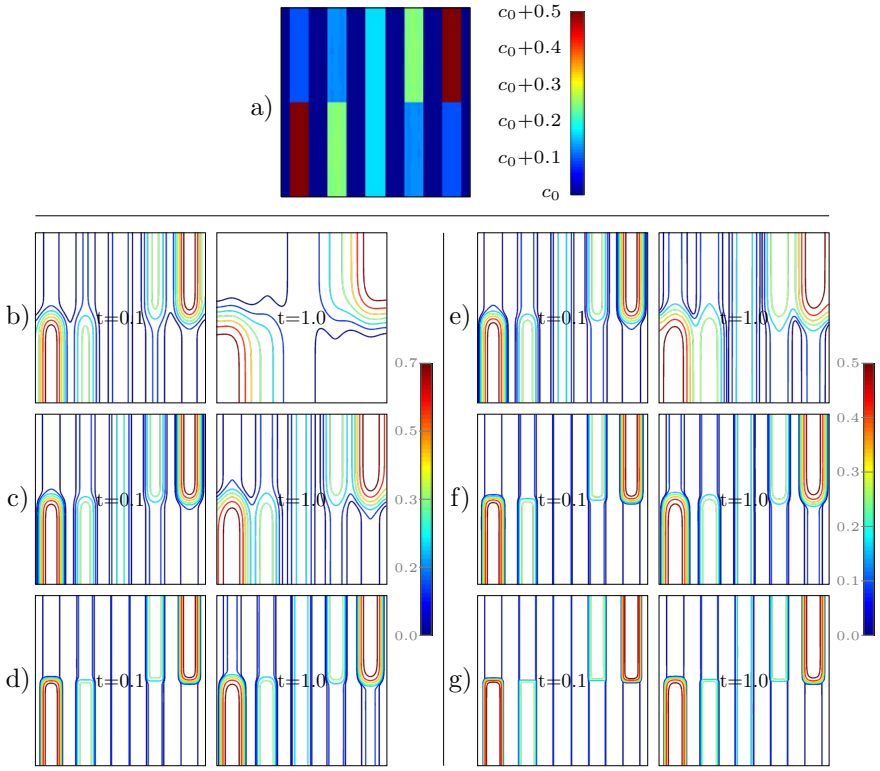


FIGURE 6.4. *Plot a) depicts a color shading of the initial data. Below, isolines of reduced solutions are given at time instances* $t = 0.1$ *and* $t = 1.0$ *for different parameter vectors: b)* $\boldsymbol{\mu} = (1, 0.01, 0.2)$*, c)* $\boldsymbol{\mu} = (2, 0.01, 0.2)$*, d)* $\boldsymbol{\mu} = (4, 0.01, 0.2)$*, e)* $\boldsymbol{\mu} = (1, 0.01, 0.0)$ *, f)* $\boldsymbol{\mu} = (2, 0.01, 0.0)$ *and g)* $\boldsymbol{\mu} = (4, 0.01, 0.0)$.

none outside. Furthermore, Figure 6.4 vividly illustrates the nonlinear effects, as the diffusion is larger (more contour lines) in the bars with high initial concentration. An exception, of course, are the reduced solutions in the upper row modelling linear diffusion where the diffusivity stays the same globally. For the discretization, we chose again the finite volume scheme from §3.1 on a $150 \times 150$ grid for decomposing $\Omega$. The global CFL condition then holds with $K = 120$ time steps. The diffusivity is discretized implicitly, such that its nonlinearities are to be resolved with the Newton-Raphson method.

**Offline phase.** Like in the previous example, we compute the reduced basis spaces on a workstation computer with eight cores each running at 2.83 GHz with Algorithms 2.1 and 4.1 using the parallel hardware architecture where possible. The empirical interpolation algorithm takes 7.5 hours until it has reached the maximum number of basis functions $M_{\max} = 250$, and the reduced basis space generation terminates after 5 hours and $N_{\max} = 50$ generated reduced basis functions.

Figure 6.6 consists of two plots illustrating the error decrease of the interpolation error respectively of the reduced simulations for growing bases dimensions. The right hand side plot shows the maximal *estimated* error in the training set $M_{\text{train}}$, because for efficiency reasons the a posteriori error estimator from §5 is used as an indicator for new reduced basis function during the "POD-greedy" search algorithm. The actual

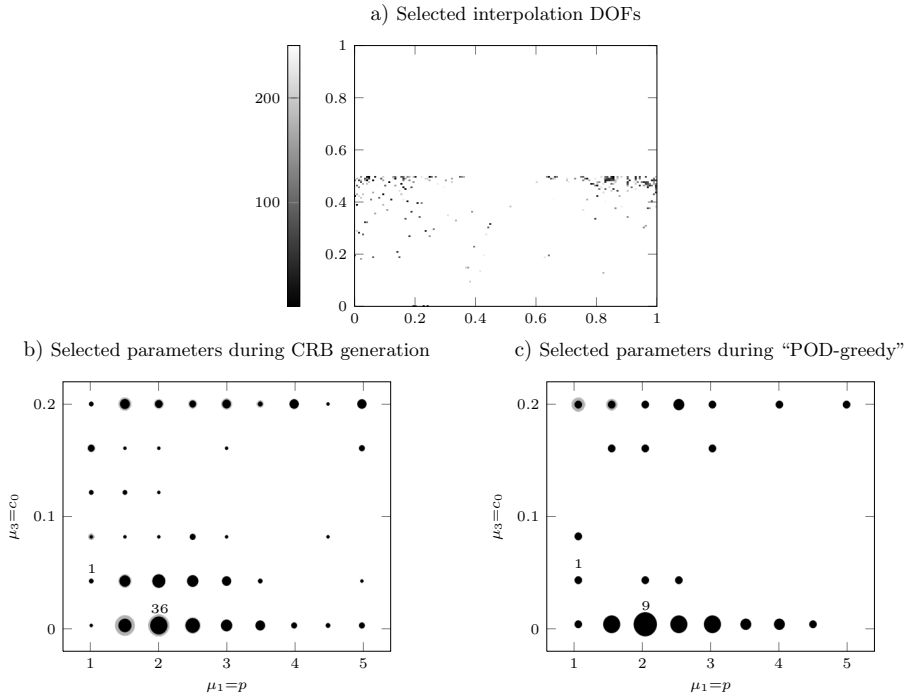


FIGURE 6.5. *Illustration of reduced basis space algorithms: Plots b) and c) are bubble plots counting selected parameters during collateral reduced basis respectively reduced basis extension. The black (●) and the grey (●) circles' radius scale with the number of selected parameters of type* $(\mu_1, 0.01, \mu_3)$ *respectively* $(\mu_1, \mu_2, \mu_3)$ *with* $\mu_2 \in \{0.25, 0.5, 0.75, 1\}$

difference between reduced and detailed simulations should therefore be even less, and its error curve is expected to be strictly monotonically decreasing. We refer to the next section for more details on the experimental evaluation of the a posteriori error estimator.

As the initial data function is point symmetric in the domain's midpoint, the selected empirical interpolation DOFs reveal an obvious model reduction pattern like for the previous Burger's problem setting. In this special case, Figure 6.5a) shows that all the midpoints at which the selected DOF functionals evaluate, lie in the lower half of the domain.

The two bubble plots in Figure 6.5 depict another aspect of model order reduction by the intelligent search for reduced basis spaces. They illustrate which and how often detailed solution snapshots from the training sets are selected for basis enrichment. We nicely observe two facts: First, solutions that show a complex evolution over time, are selected more frequently until they are approximated well enough, and second for the more "static" solutions, few or even zero snapshots are sufficient, because these can be approximated by linear combinations of other basis functions.

**Online phase.** To assess the reduced simulations quality, we proceed exactly as we did in the previous section for the Burger's problem. We again pick a test sample $M_{\text{test}} \subset \mathcal{P}$ of 20 randomly chosen values from the parameter space, measure the error $\|u_h(\boldsymbol{\mu}) - u_{\text{red}}(\boldsymbol{\mu})\|_{L^\infty(L^2(\Omega);[0,T_{\max}])}$ for all $\boldsymbol{\mu} \in M_{\text{test}}$ and compare the computation times of detailed and reduced simulations. Results for different magnitudes for the

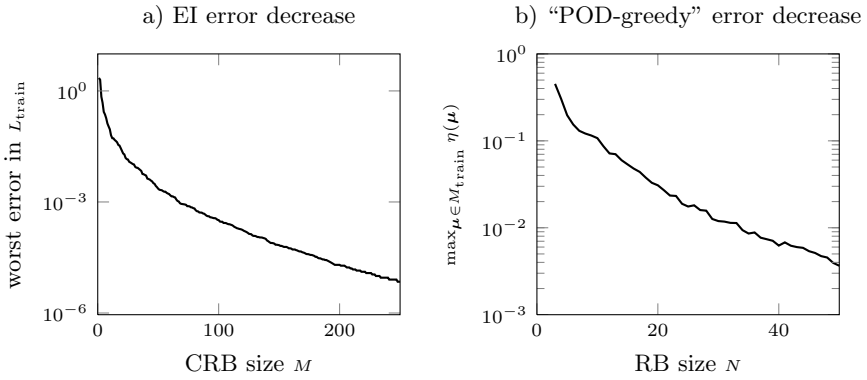


FIGURE 6.6. *Error decrease during a) CRB generation and b) "POD-greedy" algorithm.*

| Simulation | Dimensionality | Runtime[s] | Error |
|---|---|---|---|
| Detailed | H=22500 | 605.66 | – |
| Reduced | N=15, M=75 | 5.01 | $4.93 \cdot 10^{-3}$ |
| Reduced | N=30, M=150 | 7.14 | $1.73 \cdot 10^{-3}$ |
| Reduced | N=40, M=200 | 8.27 | $8.53 \cdot 10^{-4}$ |
| Reduced | N=50, M=250 | 9.78 | $7.59 \cdot 10^{-4}$ |

TABLE 6.2

*Runtime comparison for detailed simulation with reduced simulations of varying reduced dimensionalities. The runtimes and errors are averaged over a test sample of size* 20*.*

reduced bases dimensions $M$ and $N$ are shown in Table 6.2. Note, that the runtimes are averaged over the test parameter set, and actually show a high deviation from this mean by factors up to 10, because the number of Newton steps that are needed to proceed between time-steps varies noticeably. For linear problems one Newton step is enough, whereas up to a maximum of 20 Newton steps for more difficult parameters are necessary. Consequently, the acceleration factors for reduced simulations with maximum reduced basis dimensions also differ between 25 and 110.

**6.3. A posteriori error estimator.** The a posteriori error estimator from §5 has two main purposes: It should first give a tight and rigorous bound on the real error made through the model order reduction, and second improve the run-time of POD-greedy algorithms by providing an efficient and trust-worthy error indicator. In this section, we evaluate how good both these tasks are fulfilled.

In a first test, we check the efficiency of the error estimator

$$\lambda(\boldsymbol{\mu}) := \frac{\eta^K(\boldsymbol{\mu})}{\|u_h(\boldsymbol{\mu}) - u_{\text{red}}(\boldsymbol{\mu})\|} \tag{6.5}$$

for a random sample of 20 parameters and different values for the extra collateral basis functions $M'$ used to estimate the interpolation error. We expect $\lambda(\boldsymbol{\mu})$ to be greater than one, meaning the estimator is rigorous, i.e. does not underestimate the real error. On the other hand, it is desirable that the efficiency is very close to one, of course.

We make use of the above described porous medium problem, and compute the efficiency for a test sample of 20 randomly chosen parameters. For the computation of

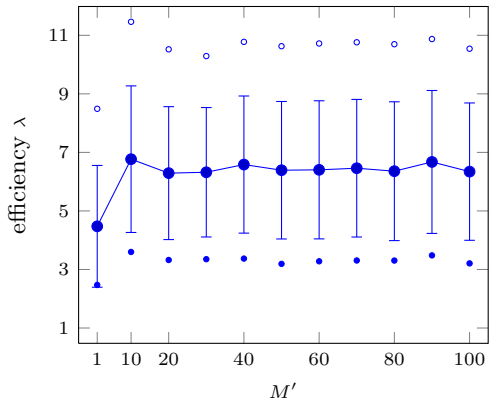


FIGURE 6.7. *Error bar plot showing mean and standard deviation of error estimator efficiency over a sample of* 20 *random parameters for different values of* $M'$. *The dots indicate the minimum* (●) *and maximum* (○) *efficiency.*

the error estimator, the Lipschitz-constant $C_I$ for the implicit discretization operator needs to be specified, which we can choose to be equal to 1 in this case. Recall our assumption, that a large enough collateral reduced basis allows interpolated operator evaluations to be almost exact. This gives rise to assess the empirical operator interpolation error with basis dimension $M$ by comparing it to the finer interpolation with basis dimension $M + M'$. One question that needs to be answered empirically here, is whether this assumption is valid and if yes, how big $M'$ needs to be chosen.

The results of our experiments are illustrated in Figure 6.7: The plot shows statistical data of the measured effectivities for different error estimators, i.e. different values for $M'$.

We observe, that the mean effectivity is slightly below 5 for $M' = 1$ and stabilizes at about 7 for small $M'$ already. The latter gives rise to our assumption that the empirical interpolation error is well approximated by a small set of extra basis functions. The number of extra basis functions should not be chosen too small, however, as the jump in the graph after $M' = 1$ indicates the first error estimator cannot fully reconstruct the interpolation error.

As the standard deviation of the error estimator's efficiency is still in a reasonable range for the sample parameters in this test, we can expect the estimator to have a good qualification as an error indicator for the "POD-greedy" algorithm. This is checked in further test runs where the "POD-greedy" algorithm is run several times with different indicators for the greedy search. The result are shown in Figure 6.8. The plot on left hand side, shows the maximum error for all parameters from the trainings set at each reduced basis extension step during the "POD-greedy" search algorithm. Here, the black line depicts a reference run of the basis extension algorithm with the "true" error as an indicator. We observe, that the error decrease for the other runs lies close to the reference line and shows no qualitative deviation of the generated reduced basis - no matter what value has been chosen for $M'$. This confirms our assumption that the estimator is a valid error indicator for the greedy search. Furthermore, the right hand side plot illustrating the error indicator decrease, confirms the previously observed result, that the error is overestimated by about one order of magnitude. We also see nicely, that the line for $M' = 1$ lies slightly beneath the more detailed estimator's curves which run almost one upon the other.

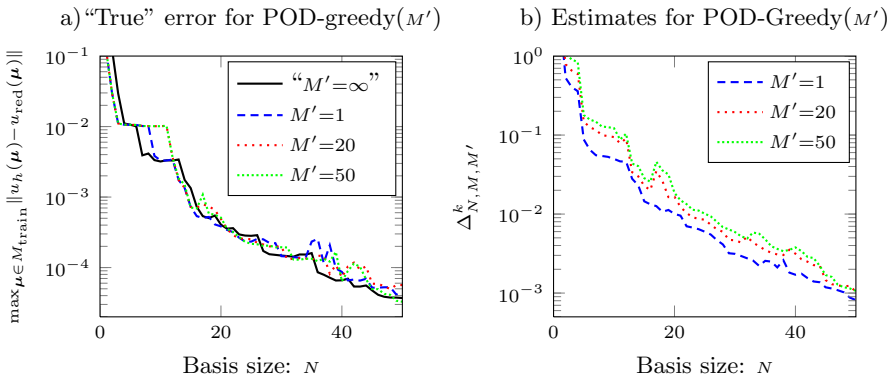


FIGURE 6.8. *Comparison of a) error decrease and b) estimated error decrease during POD-Greedy with different error indicators selecting the worst approximated trajectories (c.f. Algorithm 4.1). The error indicators vary in the number of collateral reduced basis functions $M'$ used in order to approximate the empirical interpolation error.*

**7. Outlook and conclusion.** With sophisticated parametrized evolution problems in mind, we developed an empirical operator interpolation technique for nonlinear discrete operators and their directional derivatives. This allows to apply the reduced basis framework to nonlinear evolution problems. We exemplified the approach for finite volume approximations where Newton's method is used to solve the resulting nonlinear systems. We derived a new a posteriori error estimator for the error between reduced and detailed simulations, and showed that it helps to accelerate the reduced basis generation during the offline phase.

We demonstrated, that the reduced basis methodology respectively the interpolation procedure is able to detect spatial redundancy. In the given examples, it realized not only spatial compression but even symmetry detection and dimensionality reduction. In our experiments, the reduced models have shown an acceleration of at least one order of magnitude, but we could also demonstrate that this factor grows with the problem size. The reduced basis framework developed in this paper, allows to consider numerical schemes with all kind of implicit and explicit discretizations. For implicit schemes the acceleration effect is stronger than for explicit methods, because of their squared complexity in the number of degrees of freedom $\mathcal{O}(H^2)$.

Future work will deal with more complex problems. As those usually depend on the coupling of different equations or very high dimensional parametrizations, more sophisticated basis generation algorithms are necessary. Here, we can improve the methods by more intelligent search algorithms in the parameter space and by producing smaller bases for reasonably selected subsets of the parameter space or the time interval as proposed in [8, 12, 13].

## REFERENCES

[1] http://morepas.org.
[2] M. Barrault, Y. Maday, N.C. Nguyen, and A.T. Patera. An 'empirical interpolation' method: application to efficient reduced-basis discretization of partial differential equations. *C. R. Math. Acad. Sci. Paris Series I*, 339:667–672, 2004.
[3] C. Canuto, T. Tonn, and K. Urban. A-posteriori error analysis of the reduced basis method for non-affine parameterized nonlinear pde's. *SIAM J. Numer. Anal.*, 47(e):2001–2022, 2009.

[4] J. Carrillo. Entropy solutions for nonlinear degenerate problems. *Arch. Ration. Mech. Anal.*, 147(4):269–361, 1999.
[5] S. Chaturantabut and D.C. Sorensen. Nonlinear model reduction via discrete empirical interpolation. *SIAM J. Sci. Comput.*, 32(5):2737–2764, 2010.
[6] P.G. Ciarlet. *The finite element method for elliptic problems*. North-Holland, 1978.
[7] M. Drohmann, B. Haasdonk, and M. Ohlberger. Reduced basis method for finite volume approximation of evolution equations on parametrized geometries. In *Proceedings of ALGORITMY 2009*, pages 111–120, 2008.
[8] J. Eftang, D. Knezevic, and A.T. Patera. An hp certified reduced basis method for parametrized parabolic partial differential equations. *SIAM J. Sci. Comput.*, accepted for publication, 2009.
[9] M.A. Grepl. *Reduced-basis Approximations and a Posteriori Error Estimation for Parabolic Partial Differential Equations*. PhD thesis, Massachusetts Institute of Technology, May 2005.
[10] M.A. Grepl, Y. Maday, N.C. Nguyen, and A.T. Patera. Efficient reduced-basis treatment of nonaffine and nonlinear partial differential equations. *M2AN, Math. Model. Numer. Anal.*, 41(3):575–605, 2007.
[11] M.A. Grepl and A.T. Patera. A posteriori error bounds for reduced-basis approximations of parametrized parabolic partial differential equations. *M2AN, Math. Model. Numer. Anal.*, 39(1):157–181, 2005.
[12] B. Haasdonk, M. Dihlmann, and M. Ohlberger. A training set and multiple bases generation approach for parametrized model reduction based on adaptive grids in parameter space. Technical report, University of Stuttgart (submitted), April 2010.
[13] B. Haasdonk and M. Ohlberger. Adaptive basis enrichment for the reduced basis method applied to finite volume schemes. In *Proc. 5th International Symposium on Finite Volumes for Complex Applications*, pages 471–478, 2008.
[14] B. Haasdonk and M. Ohlberger. Reduced basis method for explicit finite volume approximations of nonlinear conservation laws. In *Proc. 12th International Conference on Hyperbolic Problems: Theory, Numerics, Application*, 2008.
[15] B. Haasdonk and M. Ohlberger. Reduced basis method for finite volume approximations of parametrized linear evolution equations. *M2AN, Math. Model. Numer. Anal.*, 42(2):277–302, 2008.
[16] B. Haasdonk, M. Ohlberger, and G. Rozza. A reduced basis method for evolution schemes with parameter-dependent explicit operators. *Electron. Trans. Numer. Anal.*, 32:145–161, 2008.
[17] K.H. Karlsen and N.H. Risebro. On the uniqueness and stability of entropy solutions of nonlinear degenerate parabolic equations with rough coefficients. *Discrete Contin. Dyn. Syst.*, 9(5):1081–1104, 2003.
[18] D. Kröner. *Numerical Schemes for Conservation Laws*. John Wiley & Sons and Teubner, 1997.
[19] Y. Maday. Reduced basis method for the rapid and reliable solution of partial differential equations. In European Mathematical Society, editor, *Proceedings of International Conference of Mathematicians*, pages 1–17, 2006.
[20] N. C. Nguyen, G. Rozza, and A.T. Patera. Reduced basis approximation and a posteriori error estimation for the time-dependent viscous burgers' equation. *Calcolo*, 46(3):157–185, 2009.
[21] A.T. Patera and G. Rozza. *Reduced Basis Approximation and a Posteriori Error Estimation for Parametrized Partial Differential Equations*. MIT, 2007. Version 1.0, Copyright MIT 2006-2007, to appear in (tentative rubric) MIT Pappalardo Graduate Monographs in Mechanical Engineering.
[22] G. Rozza. *Shape design by optimal flow control and reduced basis techniques: Applications to bypass configurations in haemodynamics*. PhD thesis, École Polytechnique Fédérale de Lausanne, November 2005.
[23] K. Veroy, C. Prud'homme, and A.T. Patera. Reduced-basis approximation of the viscous Burgers equation: rigorous a posteriori error bounds. *C. R. Math. Acad. Sci. Paris Series I*, 337:619–624, 2003.

Martin Drohmann
University of Münster,
Institute of Computational and Applied Mathematics,
Einsteinstr. 62,
48149 Münster,
Germany
**E-Mail:** mdrohmann@uni-muenster.de

Bernard Haasdonk
University of Stuttgart,
Institute of Applied Analysis and Numerical Simulation,
Pfaffenwaldring 57
70569 Stuttgart
Germany
**E-Mail:** haasdonk@mathematik.uni-stuttgart.de

Mario Ohlberger
University of Münster,
Institute of Computational and Applied Mathematics,
Einsteinstr. 62,
48149 Münster,
Germany
**E-Mail:** mario.ohlberger@math.uni-muenster.de

## Erschienene Preprints ab Nummer 2010/001

Komplette Liste: `http://preprints.ians.uni-stuttgart.de`

2010/001 *Kaltenbacher, M., Shevchenko, I., Wohlmuth, B. I.:* Investigation of heat generation by acoustic waves

2010/002 *Surulescu, C., Surulescu, N.:* On two approaches to a multiscale model for bacterial chemotaxis

2010/003 *Kelkel, J., Surulescu, C.:* A multiscale approach to cell migration in tissue networks

2010/004 *Dressel, A., Rohde, C.:* A generalized Riemann problem for two-phase fluids with curvature-driven phase boundaries

2010/005 *Feistauer, M., Sändig, A.-M.:* Graded Mesh Refinement and Error Estimates of Higher Order for DGFE-solutions of Elliptic Boundary Value Problems in Polygons

2010/006 *Dihlmann, M., Haasdonk, B., Ohlberger, M.:* A Training Set and Multiple Bases Generation Approach for Parametrized Model Reduction Based on Adaptive Grids in Parameter Space

2010/007 *Hager, C., Hauret, P., Le Tallec, P., Wohlmuth, B. I.:* Overlapping domain decomposition for multiscale dynamic contact problems

2010/008 *Kutter, M., Sändig, A.-M.:* Modeling of ferroelectric hysteresis as variational inequality

2010/009 *Märkl, C., Surulescu, C.:* Mathematical analysis and numerical simulations for a system modeling acid-mediated tumor cell invasion

2010/010 *Dreyer, W., Giesselmann, J., Kraus, C., Rohde, C.:* Asymptotic Analysis for Korteweg Models

2010/011 *Steinhorst, P., Sändig, A.-M.:* Reciprocity principle for the detection of planar cracks in anisotropic elastic material

2010/012 *Drohmann, M., Haasdonk, B., Ohlberger, M.:* Reduced Basis Approximation for Nonlinear Parametrized Evolution Equations based on Empirical Operator Interpolation